iScience

Article

Bivalent SMAC mimetic APG-1387 reduces HIV reservoirs and limits viral rebound in humanized mice

Graphical abstract

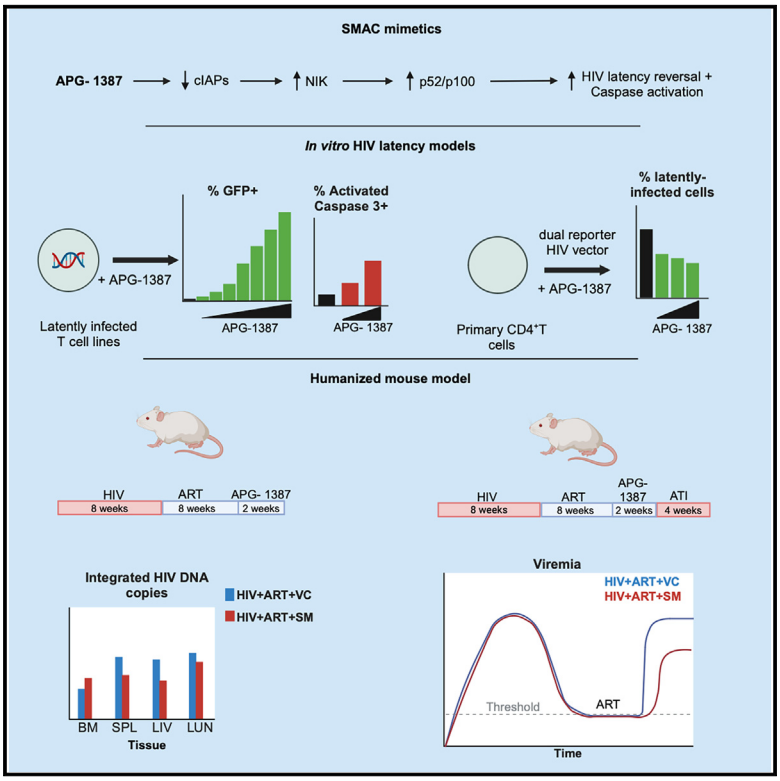

Highlights

- APG-1387 reactivates HIV expression and enhances caspase 3 levels in latent cells
- The compound does not affect global T cell proliferation or activation in hu-BLT mice
- APG-1387 reduces latently infected cells in tissues of ART-suppressed hu-BLT mice
- Viral rebound upon treatment interruption is lowered in APG-1387-treated hu-mice

Authors

Jaspreet Jain, Tram N.Q. Pham, Sharmin Begum, ..., Élie Haddad, Yifan Zhai, Éric A. Cohen

Correspondence

eric.cohen@ircm.qc.ca

In brief

Immunology; Virology; Natural sciences; Biological sciences

Jain et al., 2024, iScience *27*, 111470
December 20, 2024
https://doi.org/10.1016/j.isci.2024.111470

CellPress

iScience

CellPress
OPEN ACCESS

Article

Bivalent SMAC mimetic APG-1387 reduces HIV reservoirs and limits viral rebound in humanized mice

Jaspreet Jain,[1,2,10] Tram N.Q. Pham,[1,3,10] Sharmin Begum,[1,2] Maria Carmen Romero-Medina,[1,3] Nicolas Bellini,[1,3] Yuanyi Li,[4] Frédéric Dallaire,[1] Kathie Béland,[4] Natasha Patey,[4,5] Jean V. Guimond,[6] Élie Haddad,[3,4,7] Yifan Zhai,[8,9] and Éric A. Cohen[1,3,11,*]

[1]Institut de Recherches Cliniques de Montréal (IRCM), Montréal, QC H2W 1R7, Canada
[2]Division of Experimental Medicine, Faculty of Medicine and Health Sciences, McGill University, Montréal, QC H4A 3J1, Canada
[3]Department of Microbiology, Infectiology and Immunology, Université de Montréal, Montréal, QC H3T 1J4, Canada
[4]CHU Sainte-Justine Azrieli Research Center, Montréal, QC H3T 1C5, Canada
[5]Department of Pathology and Cellular Biology, Université de Montréal, Montréal, QC H3T 1J4, Canada
[6]Centre de Santé et de Services Sociaux Jeanne-Mance, Montréal, QC H2X 1K6, Canada
[7]Department of Pediatrics, Université de Montréal, Montréal, QC H3T 1J4, Canada
[8]Ascentage Pharma (Suzhou) Co., Ltd., Suzhou, Jiangsu 215000, China
[9]Ascentage Pharma Group, Rockville, MD 20850, USA
[10]These authors contributed equally
[11]Lead contact
*Correspondence: eric.cohen@ircm.qc.ca
https://doi.org/10.1016/j.isci.2024.111470

SUMMARY

Latent viral reservoirs (VRs) represent a main barrier to HIV cure. Thus, developing new approaches that can purge and eliminate VRs paves the path toward achieving an HIV-1 cure. APG-1387, a bivalent SMAC mimetic (SM), efficiently reactivates latent HIV expression in T cell line models and enhances active caspase 3 expression, a condition that typically leads to apoptosis. In primary CD4$^+$ T cells infected with a dual reporter-encoded HIV, APG-1387 decreases latently infected cells without a notable effect on productively infected cells. In virally suppressed humanized (hu)-BLT mice, APG-1387 augments cell-associated viral RNA and potently reduces HIV DNA-containing cells without modulating T cell activation or proliferation. Upon antiretroviral therapy (ART) interruption, HIV rebound was decreased in APG-1387-treated humanized mice (hu-mice), and the viremia maintained at levels below that of pre-ART. Thus, the ability of APG-1387 to affect VRs and decrease viral rebound highlights the potential of bivalent SMs in HIV cure strategies.

INTRODUCTION

Antiretroviral therapy (ART) has been highly effective at suppressing human immunodeficiency virus (HIV) replication, thus significantly reducing disease progression and mortality in infected individuals. However, ART is not curative and does not meaningfully impact persistent viral reservoirs (VRs) of latently infected cells that comprise CD4$^+$ T cells and myeloid cells.[1–3] Indeed, upon antiviral treatment interruption (ATI), the virus quickly rebounds after several weeks, highlighting how the presence of VRs obviates an HIV cure.[4–6] Therefore, eliminating or controlling VRs remains an unwavering priority for HIV cure research. In this context, the aim of the "shock-and-kill" strategy is to reactivate latently infected cells with latency reversal agents (LRAs) and render them vulnerable to cell death or clearance by the immune system.[7,8]

Previously reported approaches to HIV reactivation, including protein kinase C (PRKC) agonists, histone deacetylase (HDAC) inhibitors (HDACi), and toll-like receptor (TLR) agonists,[9] have been highly effective in *in vitro* models of latency, but their efficacy is only moderate when tested *in vivo*.[10–13] Moreover, by broadly activating cellular pathways, these compounds elicit significant proinflammatory effects or alter the function and fate of specific immune effector cells,[14,15] hence limiting their use in clinical settings.[16–19] Similarly, promising candidates such as bryostatin-1 and analogs, phorbol esters, and phosphatidylethanolamine binding protein 1 (PEBP1) agonists reactivate HIV via activation of the canonical nuclear factor kappa B (NFKB) pathway,[13,20] inadvertently leading to uncontrolled cytokine release and overt T cell activation.[21,22] Consequently, there is a need to develop alternative approach(es) that can reactivate latent reservoirs and eliminate infected cells without triggering systemic activation, inflammation, or impairment of immune clearance mechanisms. In this regard, small molecules known as mimetics of the second mitochondrial activator of caspases (SMAC mimetics [SMs]) were originally developed as cancer therapeutics. They have received increasing recognition because they specifically activate the non-canonical NFKB

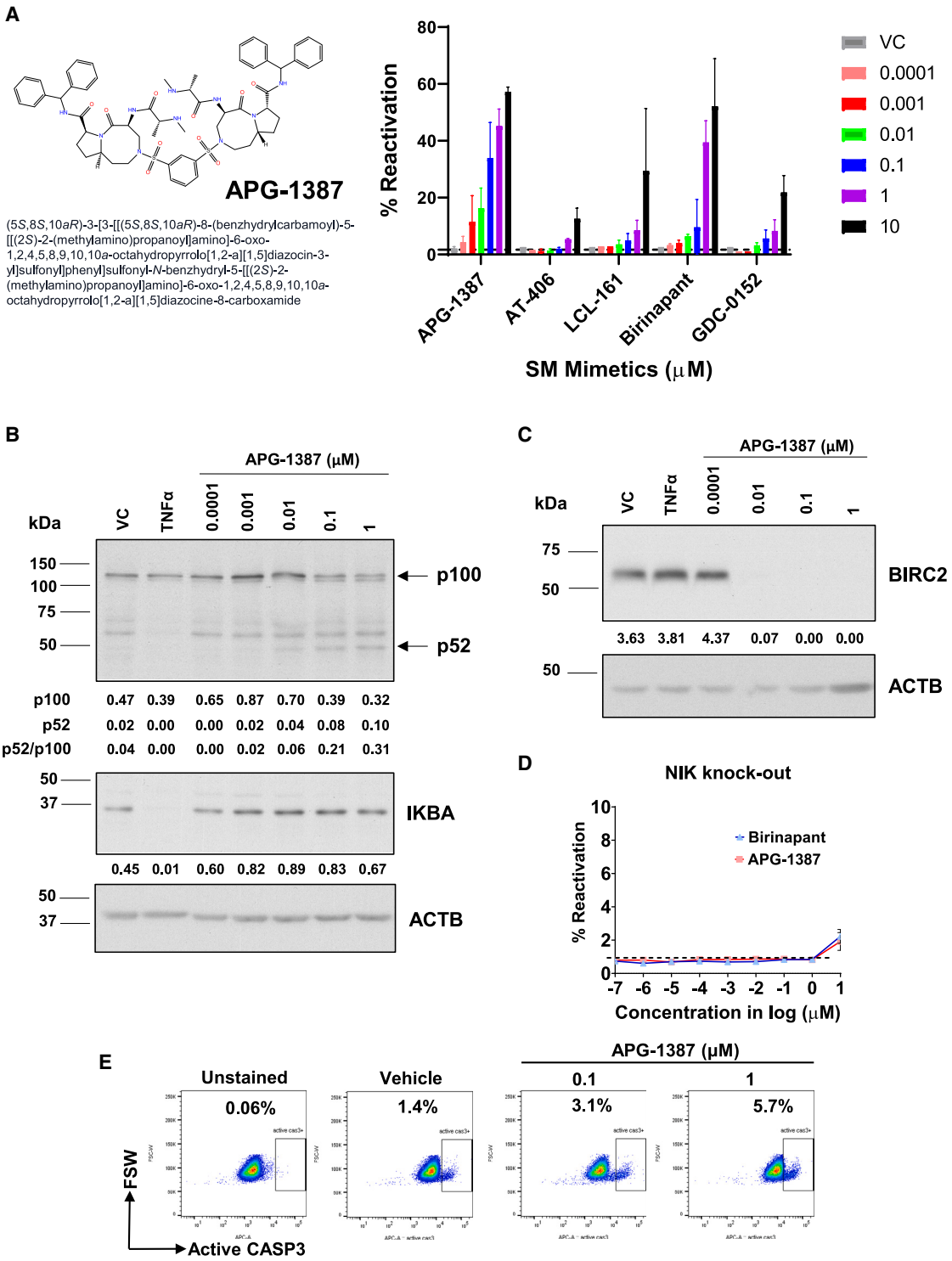

Figure 1. SMs reactivate HIV-latently infected model T cells via activation of the non-canonical NFKB pathway and lead to degradation of IAPs

(A) Left panel: Chemical structure of APG-1387 with the IUAPC nomenclature. Right panel: HIV reactivation in latently infected 2D10 cells, as measured by the percentage of cells expressing GFP, 48 h after treatment with increasing concentrations (0.1 nM–10 μM) of monovalent and bivalent SMs. Data are represented as mean ± SD from two experiments (n = 2). The dotted line is the level of reactivation in vehicle control (DMSO)-treated cells.

(B) Immunoblots for 2D10 cells treated with vehicle, TNF (an activator control of the canonical NFKB pathway, 10 ng/mL), or different concentrations of APG-1387. Expression of the indicated markers of non-canonical NFKB (p100 and p52) and canonical NFKB (IKBA) pathways was determined. Shown is a

(legend continued on next page)

pathway,[23–25] which naturally exhibits higher functional selectivity and more confined proinflammatory effects compared to the canonical NFKB pathway.[24,26]

Engagement of the non-canonical NFKB pathway by SMAC leads to degradation of cellular inhibitor of apoptosis (cIAP), accumulation of NFKB-inducing kinase (NIK), and activation of component of inhibitor of NFKB kinase complex (CHUK) homodimer, culminating in cleavage of inactive NFKB2 p100 to active p52.[26] An association between RELB and p52 induces expression of target genes[27] and, in the context of HIV, the pathway reactivates latently infected VRs.[20] The non-canonical NFKB pathway can also be triggered by signaling intermediates of the apoptosis cascade. In fact, cleavage of SMAC/DIABLO exposes the N-terminal motif Ala-Val-Pro-Ile, which binds specifically to baculovirus intermediate repeat domains 2 and 3 of IAP proteins. These proteins in turn trigger downstream events that ultimately lead to degradation of baculoviral IAP repeat containing 2 (BIRC2, also known as cIAP1) and baculoviral IAP repeat containing 3 (BIRC3, also known as cIAP2)[28] and potentiation of apoptosis.[29] The unique ability of SMAC to degrade IAPs and activate apoptosis pathway(s) makes SMs interesting candidates in the field of HIV cure research[30,31] because latently infected $CD4^+$ T cells display aberrant expression of cell survival factors, including XIAP, BIRC2 and BCL2.[8,32] Pharmacological activation of the non-canonical NFKB pathway by SMs was recently found to induce on-ART plasma viremia in animal models of HIV latency,[24,25] underscoring the potential of this class of molecules as LRAs. However, it remains unclear whether induction of HIV expression by SMs leads to a reduction of VRs in lymphoid and non-lymphoid tissues of animal models.

In this study, we show that bivalent APG-1387, currently in clinical development in the oncology field, activates the non-canonical NFKB pathway and hence, is a potent LRA. By degrading IAPs, this compound also induces the expression of active caspase 3 (CASP3), a key component of the execution phase of apoptosis, in latently infected cells. Likewise, in primary $CD4^+$ T cells infected with a dual reporter-encoded HIV, APG-1387 reduces the level of latent cells without notably affecting the productively infected pool. Accordingly, *in vivo* treatment with APG-1387 could reactivate expression of latent viruses and was found to meaningfully reduce the integrated HIV-DNA level in tissues of ART-suppressed humanized bone marrow liver thymus (BLT) mice, without assessable immunotoxicity. Upon ART interruption, APG-1387-treated mice rebounded more slowly and to a lower set point. Overall, the study demonstrates that APG-1387 has the capacity to not only reverse HIV latency but also potentiate cell apoptosis, thus supporting the notion that bivalent SMs could be harnessed to reduce VRs without causing generalized T cell activation.

RESULTS

APG-1387 induces HIV intracellular reactivation and enhances expression of active caspase-3 in $CD4^+$ T cell models of latency

APG-1387 is a bivalent SM with demonstrable antitumor activity.[33] However, it is not known whether this compound can reactivate latent HIV and/or sensitize latently infected or reactivated cells to death. Hence, we first assessed HIV reactivation by APG-1387 in 2D10 cells, a latently infected Jurkat T cell line carrying a lentiviral vector that expresses Tat H13L and Rev *in cis* and a short-lived green fluorescent protein in place of Nef,[34] and compared it to that of other SMs known to have latency-reversing activity. Indeed, bivalent SMs such as APG-1387 and Birinapant were more effective at inducing viral reactivation in 2D10 cells at equivalent concentrations compared to monovalent SMs GDC-0152, AT-406, and LCL-161 (Figures 1A and S1A). Subsequently, we performed the same analysis in J-lat 10.6 cells, a subclone of Jurkats that carries a single copy of an integrated full length Env-defective GFP (in place of Nef)-marked HIV.[35] When J-Lat 10.6 cells were treated with the same SMs, we observed significant viral intracellular reactivation by the bivalent SMs, thus extending the reactivation potential of APG-1387 to another $CD4^+$ T cell line model of HIV latency (Figure S1B).

Further, APG-1387 treatment led to an accumulation of p52 and simultaneous reduction of its precursor p100 (Figure 1B; Figure S1C), strongly indicating that the non-canonical NFKB pathway was activated. Unsurprisingly, stimulation with tumor necrosis factor (TNF), a quintessential activator of the canonical NFKB pathway, led to a near complete disappearance of total levels of the NFKB transcription factor inhibitor, IKBA, when compared to the untreated controls. However, no changes were noted in response to APG-1387 treatment, suggesting that the canonical NFKB pathway was not affected (Figure 1B and quantitative analysis of IKBA levels; Figure S1C). To further confirm engagement of the non-canonical NFKB pathway by APG-1387, we examined expression levels of host factors known to be downregulated upon activation of the non-canonical NFKB signaling cascade. As shown, BIRC2 was significantly depleted in APG-1387-treated cells in a concentration-dependent manner (Figure 1C, upper panel) with a complete depletion observed starting at 10 nM. Activation of the non-canonical NFKB pathway hinges on the stability of the NIK, which is downregulated by BIRC2/3.[26] The fact that APG-1387 treatment of NIK-knock-out 2D10 cells with APG-1387 did not lead to measurable viral reactivation, unless it was at a very high concentration (10 μM) and even then, the reactivation was drastically reduced, highlights the importance of the non-canonical NFKB pathway in latency reversal induced by SMs (Figure 1D).

representative blot of three experiments ($n = 3$). Numbers shown underneath the blots were obtained from densitometry analysis of immunoblot bands of protein of interest. Quantification was done separately for p100, p52, and IKBA by normalizing to the loading control actin beta (ACTB) using ImageJ software.
(C) Immunoblots of 2D10 cells treated with vehicle control, TNF, or APG-1387 probed for BIRC2 (cIAP1) expression. Shown is a representative blot from two independent experiments ($n = 2$). Quantification was done as described for Panel B.
(D) Evaluation of HIV reactivation in NIK-knockout 2D10 cells treated with AGP-1387, as was done in Panel A. Shown are results from three independent experiments ($n = 3$) using GraphPad Prism 8.0 software (data are represented as mean ± SD).
(E) Flow cytometry analysis showing the frequency of 2D10 cells expressing active (cleaved) CASP3 after 24-h treatment with APG-1387. Vehicle (DMSO only) was used as a negative control. See also Figures S1–S3.

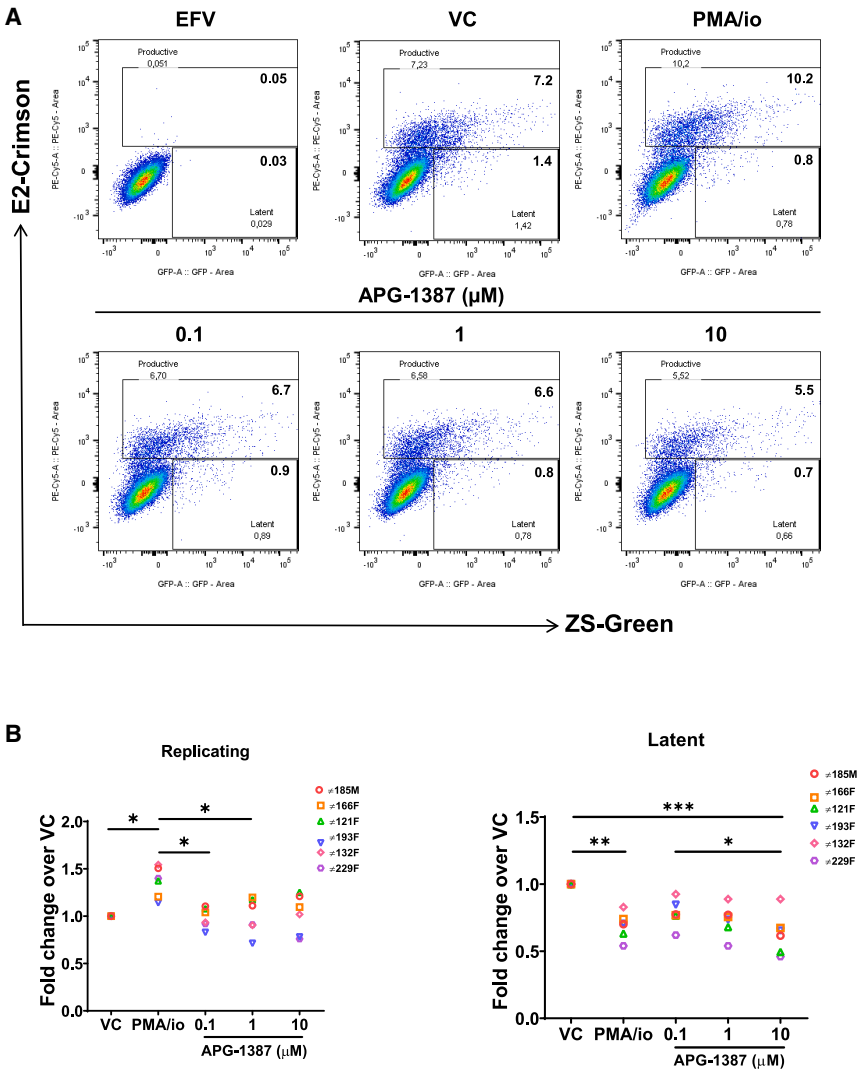

Figure 2. APG-1387 reduces the frequency of latently infected primary CD4⁺ T cells *in vitro*

(A) Flow cytometry analysis of CD4⁺ T cells infected with the HI.fate.E dual-fluorescent reporter virus, which identifies replicating and latently infected cell populations. HI.fate.E construct contains an E2 Crimson (E2-CRMZ) reporter under the control of the HIV LTR that serves as a marker for cells undergoing productive proviral expression (E2-CRMZ positive) and an EF1α promoter driving constitutive expression of a green fluorescent protein (ZS-Green) reporter. Cells harboring a latent provirus are identified as ZS-green positive/E2-CRMZ negative cells while replicating infected cells are positive for E2-CRMZ and ZS-green. Primary CD4⁺ T cells were transduced with HI.fate.E virus for 3 days and treated with DMSO, PMA/io (positive control), and APG-1387 for 24 h. Frequencies of replicating and latently infected cells were determined by flow cytometry. Efavirenz (EFV) was used to confirm the authenticity of infection.

(B) Fold change over vehicle control (VC) in replicating and latently infected cell populations. Each symbol represents a donor (n = 6 donors; M, male; F, female as indicated on the Figure). Results are shown at 24h post-APG-1387 treatment. Data are represented as median. Statistical analysis: non-parametric Friedman test followed by Dunn's multiple comparisons test *p = 0.026, **p = 0.007, ***p = 0.0004 (GraphPad Prism 8.0). Statistical significance results are as indicated on the Figure. All other pairings are not statistically significant. See also Figure S2.

Given that SMAC are activators of caspases, it is not surprising that SMs can induce apoptosis in cancer cells.[36,37] In the context of our study, we assessed whether APG-1387 could sensitize latently infected cells to apoptosis. Indeed, APG-1387 treatment led to a dose-dependent increase in the level of CASP3 in both 2D10 (Figure 1E) and J-Lat 10.6 (Figure S1D), signifying potential activation of apoptosis pathway(s). Taken together, APG-1387 is a bivalent SM, capable of efficiently reactivating HIV expression via the non-canonical NFKB pathway and enhancing the expression of active CASP3 in CD4⁺ T cell line models of viral latency.

APG-1387 reduces the frequency of latent cells without detectable viral reactivation in a primary cell model of HIV-1 latency

We next assessed whether the findings obtained in the cell lines could also be replicated in primary CD4⁺ T cells. In uninfected cells, APG-1387 indeed significantly induced BIRC2 and BIRC3 degradation, enhanced p100 processing into p52 while keeping IKBA at comparable levels, indicating a primary activation of the non-canonical NFKB pathway (Figure S2). As well, APG-1387 treatment led to a marked increase in the level of cleaved caspase 3 in both uninfected and HIV-infected CD4⁺ T cells, and the enhancement was more pronounced in infected cells compared to the uninfected (Figure S3).

To study whether APG-1387 could reactivate latent virus in primary CD4⁺ T cells and/or sensitize them to death, we took advantage of the single-cycle HI.fate.E dual reporter virus[38,39] with which latent cells (i.e., not expressing viral genes) or cells supporting viral replication (or replicating infected cells), can be readily identified by flow cytometry as only ZS-Green-positive cells or E2-Crimson positive, ZS-Green -positive/negative cells, respectively (Figure 2A). As originally reported, in this dual reporter virus, HIV LTR-directed gene expression was used as a marker for cells supporting viral replication although the virus is not replication-competent and viral particles released are not assessed.[38] As expected, pretreatment of CD4⁺ T cells with the reverse transcriptase inhibitor Efavirenz blocked infection. Phorbol-12-myristate-13-acetate (PMA) and ionomycin, which activate the canonical NFKB pathway, reduced the frequency of latently infected cells, and increased the level of cells supporting replicating virus as compared to the control. At 10 μM

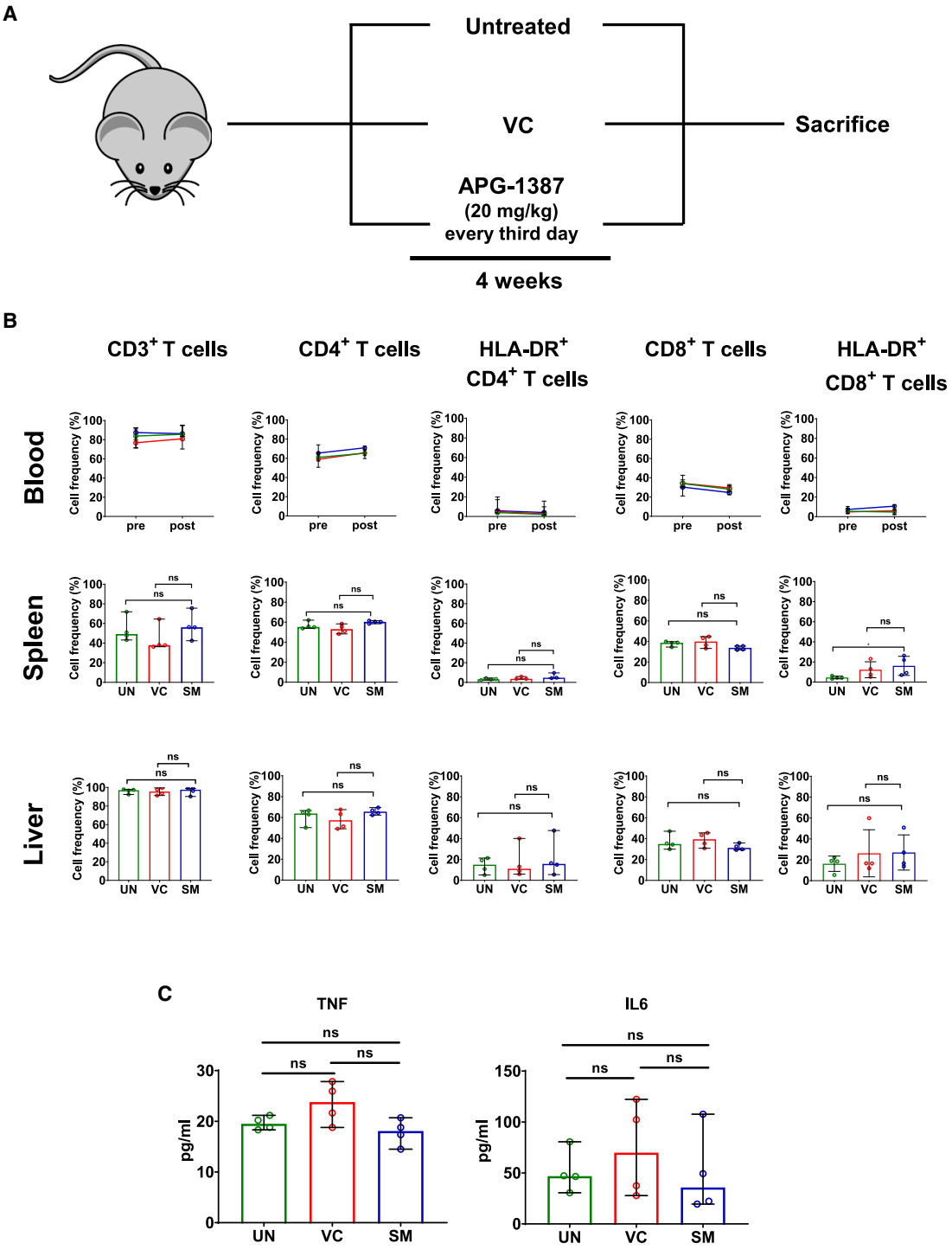

Figure 3. APG-1387 does not cause overt immunotoxicity in hu-BLT mice

(A) Experimental setup to assess effects of APG-1387 in hu-BLT mice. Uninfected mice were left untreated (UN) or treated with either vehicle control (VC) or APG-1387 (SM) for 4 weeks. Untreated mice were used to gauge the effect of the vehicle control.

(B) Shown are frequencies of HLA-DR$^+$ cells among CD4$^+$ and CD8$^+$ T cells (gated on human CD45$^+$ cells) before and after APG-1387 treatment. Data were represented as median with range. Statistical analysis: Wilcoxon matched pairs signed rank test for samples in the blood; non-parametric two-tailed

(legend continued on next page)

APG-1387, the latently infected cell population was decreased by at most~2-fold but the pool of cells supporting HIV LTR-directed gene expression was not significantly affected (Figures 2A and 2B), implying that APG-1387 might be more effective at targeting the latent cell population in this primary cell model. Indeed, compared to vehicle-treated cells, the decrease in the frequency of latent cells was statistically significant at 10 μM APG-1387, and such a reduction was also statistically meaningful between 0.1 μM and 10 μM (Figure 2B). In this context, our finding is consistent with that reported by others, which have shown that SMs can selectively eliminate latently infected primary cells or latent reservoirs from T cells of HIV-infected, ART-suppressed individuals, without inducing detectable viral reactivation.[23,32] We did not observe any sex-related differences, albeit there was only one male out of six subjects studied. Taken together, our data demonstrate that APG-1387 is an effective LRA in T cell lines but in primary $CD4^+$T cells, it tends to decrease the frequency of latently infected cells without noticeably causing a detectable increase in the level of cells undergoing LTR-directed gene expression.

APG-1387 is nontoxic in uninfected hu-BLT mice

To assess whether APG-1387 could be a potential LRA *in vivo*, we first performed a pharmacological analysis in uninfected hu-BLT mice to gauge any off-target effects or immune-mediated toxicity. In brief, mice were administered with APG-1387 (20 mg/kg)[40] or vehicle control every third day for 4 weeks (Figure 3A). This dosage was chosen because APG-1387 anti-tumor activity was observed at this concentration in a xenograft mouse model.[40] T cell frequency along with their activation status were monitored in the blood and other tissues before and after treatment (Figure 3B; Figure S4). As indicated, APG-1387 treatment did not lead to notable, global changes in the level of T cells. No increase in the frequency of $CD4^+$ T or $CD8^+$ T cells expressing the activation marker HLA-DR was observed in tissues of APG-1387-treated mice. Importantly, APG-1387 treatment did not increase the levels of inflammatory cytokines TNF or interleukin 6 (IL6) (Figure 3C). Taken together, these results demonstrate that APG-1387 treatment does not result in overt immunotoxicity *in vivo*.

APG-1387 reduces the frequency of latently infected cells and modestly increases HIV RNA detection in ART-suppressed hu-BLT mice

Humanized mice (hu-mice) were inoculated with HIV-1 NL4.3-ADA-GFP and at peak viremia, infected mice were treated with subcutaneous ART daily for 6 weeks. To gauge the effect of repeated administration of APG-1387 on HIV RNA and DNA levels in the context of uninterrupted ART, we treated ART-suppressed mice with at least four doses of APG-1387 (or vehicle control) over the course of two weeks (Figure 4A). Here, one mouse in the APG-1387-treated group had a viremia level above the background after the two-week treatment while the rest displayed an undetectable viremia throughout the follow-up (Figure 4B). Of note, when virally suppressed mice received a single dose of APG-1387 upon cessation of ART, plasma viral load became detectable in three out of six animals, suggesting that the activity of APG-1387 as a latency reversal agent is more apparent in this context (Figure S5).

We observed that APG-1387 treatment modestly increased the level of cell-associated HIV RNA transcripts in the lung and spleen by up to 1.7- and 2.2-fold, respectively, but not in the bone marrow or the liver (Figure 4C). Regarding the effect of APG-1387 on the level of total HIV DNA-harboring cells, we observed a trend toward a reduction in the spleen, liver and lung but not in the bone marrow (Figure 4D). For the integrated HIV DNA, the difference was noticeably more pronounced in the spleen, liver, and lung of APG-1387-treated mice (Figure 4E), and the reduction reached statistical significance (by two-tailed Mann-Whitney tests) for the spleen ($p = 0.0043$) and liver ($p = 0.0317$) tissues, but not for the lung ($p = 0.1255$). APG-1387 does not markedly affect T cells in uninfected mice (Figure 3B; Figure S4) but augments the level of active CASP3 in latent T cell lines (Figure 1E; Figure S1D). In a dual reporter virus system, it preferentially reduces the frequency of latently infected primary $CD4^+$ T cells (Figure 2). Thus, it is tempting to hypothesize that the decreased abundance of integrated HIV DNA-containing cells is due to a potential reduction in the frequency of persistent latent VRs by APG-1387.

APG-1387 does not exert overt T cell activation in ART-suppressed hu-BLT mice

Previously, it was reported that AZD5582, a bivalent SM, might induce activation and proliferation of T cells.[24] Thus, we evaluated whether APG-1387 altered the expression of marker of proliferation Ki-67 MKI67 or activation markers HLA-DR and CD69 on T cells. Here, we found no significant changes in the level of HLA-DR and CD69 in any of the tissues tested (Figures S6A and S6B). MKI67 expression was enhanced in certain organs, similar to what was reported previously.[24] However, plasma levels of proinflammatory cytokines IL6 and TNF were comparable between the two groups (Figure S6C). We found no differences in the frequency of $BCL2^+$ $CD3^+CD8^-$ T cells (i.e., $CD4^+$ T lymphocytes) in tissues of mice treated with APG-1387 (vs. vehicle control). However, consistent with earlier data obtained in the latent T cell lines (Figures 1E and S1C), the frequency of CASP3-positive CD8-T cells (i.e., $CD4^+$ T cells) was significantly higher in the bone marrow and liver cells of APG-1387-treated mice compared to vehicle-treated animals (Figure S6D).

Effects of *in vivo* and *ex vivo* treatment with APG-1387 on $CD4^+$ T cell subsets of HIV-infected mice

Having observed that APG-1387 reduced the frequency of HIV DNA-containing cells in several tissues in ART-suppressed hu-BLT mice, we next explored how APG-1387 might have affected different immune cell subsets in these animals. Various SMs

Mann-Whitney unpaired rank test for the other tissues; *$p = 0.0286$; ns, not significant. Exceptionally, the % of HLA-DR^+ $CD8^+$ T cells in the spleen was statistically significant between untreated (UN) and APG-1387 (SM) treated mice ($p = 0.0286$), but not between vehicle (VC) and APG-1387 treated animals.
(C) Plasma from untreated (UN) mice or those treated with vehicle (VC) or APG-1387 (SM) was analyzed by ELISA for TNF and IL6. In all panels, there were $n = 4$ mice per experimental group. Data were represented as median with 95% CI. Statistical analysis: non-parametric Friedman test followed by Dunn's multiple comparisons test (GraphPad Prism 8.0); ns, not significant. See also Figure S4.

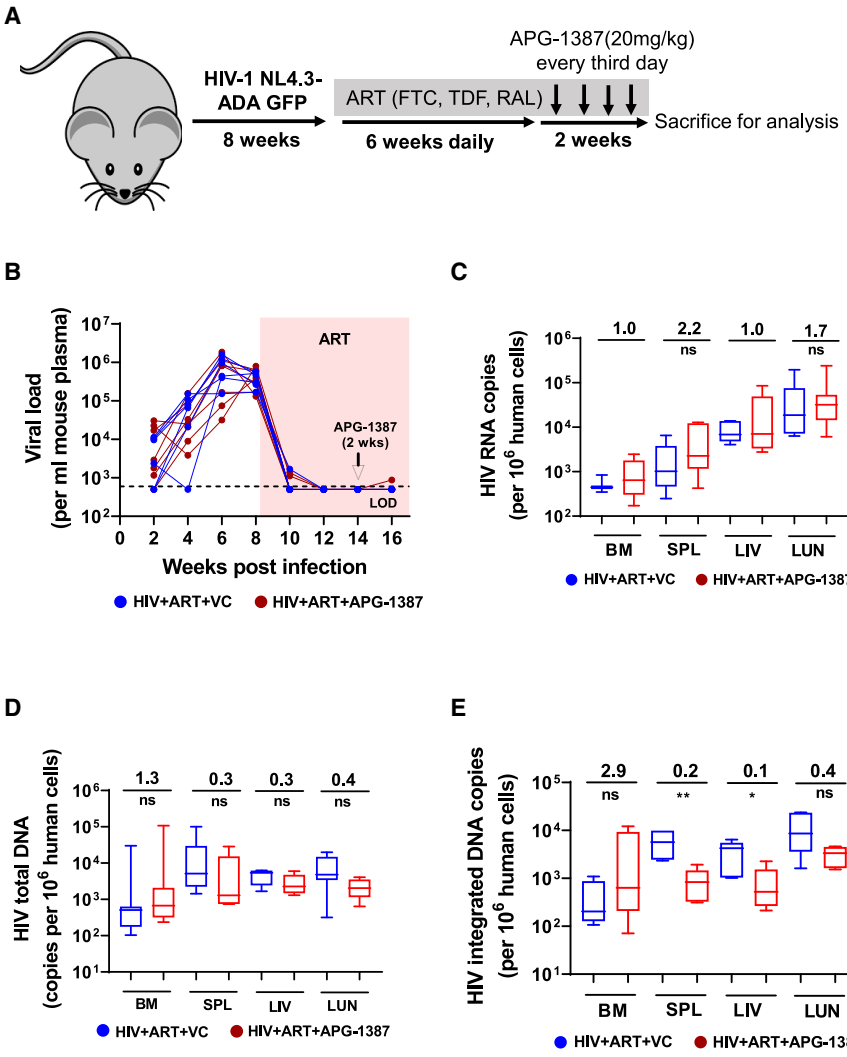

Figure 4. APG-1387 reduces the frequency of latently infected cells and modestly increases HIV RNA detection in ART-suppressed hu-BLT mice

(A) Hu-BLT mice were infected with NL4.3-ADA-GFP virus and virally suppressed with ART for 6 weeks. Thereafter, mice received four doses of either vehicle or APG-1387 in the presence of ART.

(B) Plasma viral load in mice receiving vehicle (VC, n = 6, blue lines) or APG-1387 (n = 7, red lines). Pink shading depicts the period of ART administration. The dotted line represents the limit of detection (LOD) of the assay.

(C–E) HIV-RNA (C), total HIV DNA (D) and integrated HIV-DNA (E) were analyzed in different tissues by RT-qPCR or qPCR, respectively. Box and whisker graphs indicate median, min and max values. The number on the top of the horizontal line shows the fold change in median levels of HIV RNA or HIV DNA in APG-1387- treated mice over vehicle (VC)-treated mice. Samples were analyzed in technical duplicates and there were five to seven mice per group (n = 5 to 7). For each tissue, the number of mice tested per group was between five to seven except for the bone marrow for the vehicle-treated group when there were three available. Statistical analysis: Two-tailed Mann-Whitney unpaired rank test. *p = 0.0317; **p = 0.0043; ns, not significant (GraphPad Prism 8.0). In (E), p = 0.1255 for the lung. See also Figures S5 and S6.

have been shown to inhibit Th17 function[41] or decrease Treg differentiation,[42] and because both Th17 and Tregs are known to be affected during HIV infection,[43–45] we assessed whether *in vivo* APG-1387 treatment could affect these populations. First, we found that *ex vivo* stimulation of combined PMA and ionomycin greatly improved the detection of IL17A-producing CD4$^+$ T (Th17-like cells) in splenocytes of ART-suppressed mice previously treated or not with APG-1387 (Figure 5A). However, cell activation with PMA/ionomycin did not affect the identification of forkhead box P3 (FOXP3)-expressing CD4$^+$ T cells (Figure 5B). *In vivo* treatment with APG-1387 modestly decreased the frequency of splenic Th17-like cells in ART-suppressed mice by 45% (mean 4.5 ± 1.8% in VC-treated group vs. 2.5 ± 1.3% in APG-1387-treated group) but the difference was not statistically significant (p = 0.11), possibly because of the small number of mice and variations between them (Figure 5A). In the case of FOXP3-expressing CD4$^+$ T cells, we observed no significant increase (p = 0.41) in the proportion of these cells in the APG-1387 treated group (mean 7.3 ± 1.1% in VC-treated vs. 10.7 ± 4.5% in APG-1387 treated group) (Figure 5B).

To assess whether APG-1387 targets specifically infected cells that actively express viral proteins, we performed a complementary experiment in which splenocytes from HIV-infected, ART-naïve mice were treated with APG-1387 *ex vivo* (Figures 5C and 5D). Here, exposure to APG-1387 led to a moderate decrease in the number of p24-expressing total CD4$^+$ T cells (p = 0.062) in all mice tested (n = 5). For the Th17-like and FOXP3$^+$ CD4$^+$ T cell subsets, this trend was observed in 3 of 5 mice for Th17-like CD4$^+$ T cells (p > 0.99) and 4 of 5 for the FOXP3$^+$ CD4$^+$ T cell subset (p = 0.62). Taken together, our data suggest that APG-1387 can reduce the proportion of infected CD4$^+$ T cells that are actively producing viral protein(s).

APG-1387 reduces viral rebound after ART treatment interruption

Given the effect of APG-1387 on the pool of latently infected cells in previous experiments with the dual reporter virus (Figure 2) and in virally suppressed hu-mice (Figure 4), we sought to perform an ART-treatment interruption (ATI) to assess the impact of APG-1387 on the VRs. To test our hypothesis that mice treated with APG-1387 would display a slower viral rebound upon ATI, we administered four doses of APG-1387 (or vehicle control) alongside ART to virally suppressed mice as shown in Figure 4. Two weeks thereafter, ART was removed and the mice were sacrificed after 4 weeks off ART (Figure 6A). As shown

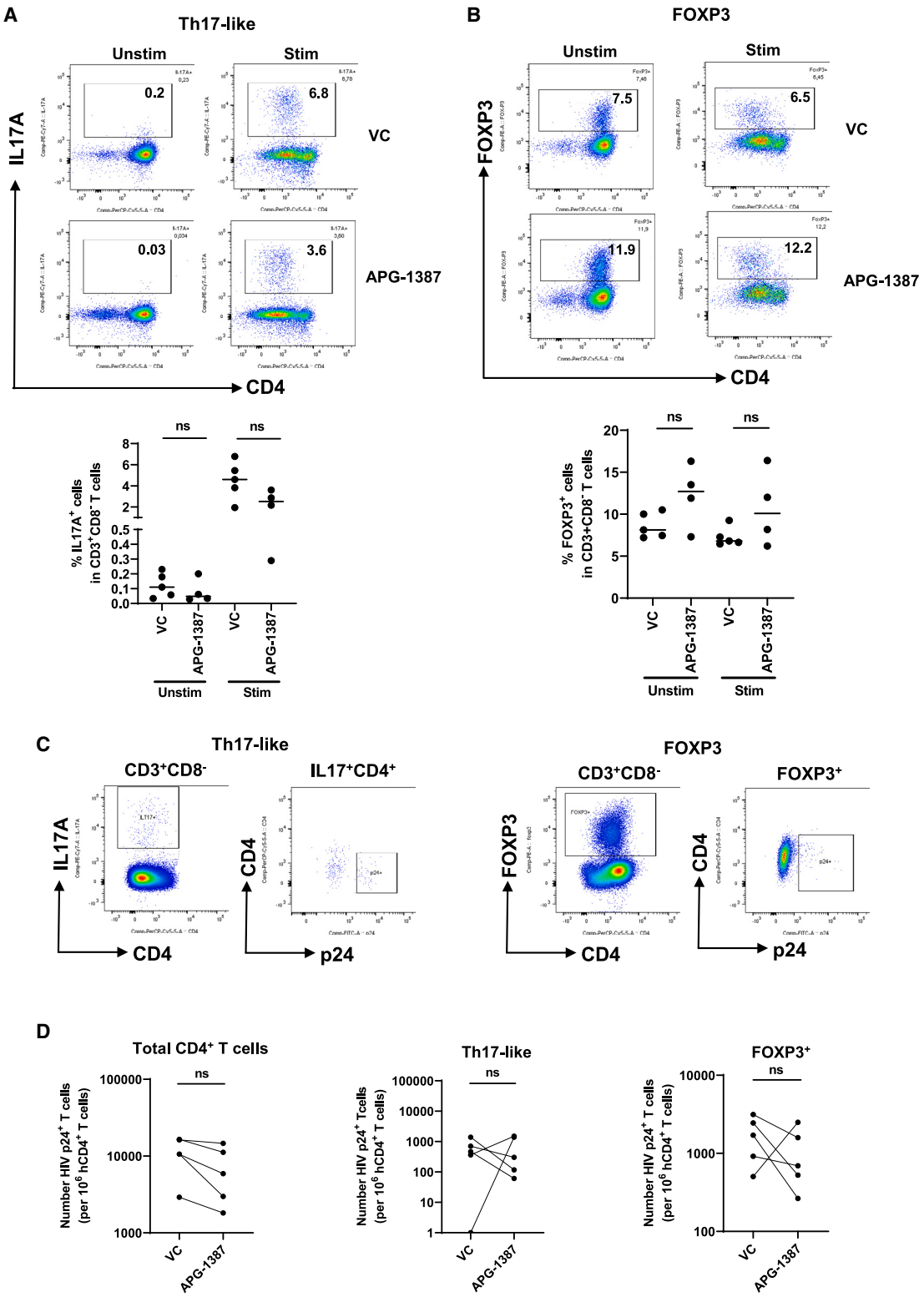

Figure 5. Effects of APG-1387 on Th17-like and FOXP3-expressing CD4⁺ T cells *in vivo* and *ex vivo*

(A and B) Spleen cells from virally suppressed, vehicle-treated (VC) or APG-1387-treated hu-BLT mice were left unstimulated (Unstim) or stimulated *ex vivo* with combined PMA and ionomycin (Stim) for up to 24h and analyzed for IL17A-producing (Th17-like) (Panel A) or FOXP3-expressing CD4⁺ T cells (Panel B). Representative flow graphs depicting the two cell subsets (gated on human CD45⁺ CD19⁻CD14⁻CD3⁺ populations) are shown on the top. Bottom panels are

(legend continued on next page)

in Figure 6B, plasma viral loads in the three APG-1387-treated mice were at least 66-fold lower than that in the control group two weeks after ART cessation (Table S1). At the end of the experiment, the viremia remained lower in APG-1387-treated mice by more than 6-fold (Table S1). Importantly, a longitudinal analysis of the viremia showed that in APG-1387-treated mice the viral rebound plateaued at a level notably lower than that pre-ART, suggesting that the size of the reservoir was affected. On this note, the data overall support the notion that APG-1387 reduces viral rebound in HIV-infected hu-mice upon ART interruption by decreasing the pool of latently infected cells that persists during ART.

DISCUSSION

Several LRAs have shown their biological activity both *in vitro* and *in vivo* but are clinically unsafe for further evaluations.[46,47] The most potent LRAs, including HDACi and protein kinase C (PRKC) agonist bryostatin-1, activate the canonical NFKB pathway,[46] causing explicit T cell activation and broad cytotoxicity, and hence eliciting significant collateral damage on host cells. Reactivation of latent HIV by PRKC agonists has recently been demonstrated to induce resistance to apoptosis, a phenomenon often associated with phosphorylation and activation of the antiapoptotic protein BCL2.[48] Thus, the failure of common LRAs such as PRKC agonists and HDACi to safely purge HIV and effectively reduce VRs in people living with HIV necessitates the development of clinical approaches to achieve an HIV cure. In this study, we demonstrate that APG-1387, a bivalent SM initially developed as a cancer therapy, can efficiently reactivate HIV in $CD4^+$ T cell line models of HIV-1 latency via a process that involves activation of the noncanonical NFKB pathway. Although this IAP antagonist modestly increases HIV RNA detection in virally suppressed hu-mice, it has the capability to reduce both the frequency of latently infected cells and the level of viral rebound upon ART treatment interruption. Indeed, APG-1387 treatment enhances the expression of caspase-3, a marker of apoptosis, in latently infected cells from T cell lines or in T cells from certain tissues of virally suppressed hu-mice. In the context of productive infection, *in vitro* stimulation with APG-1387 also enhanced cleavage of CASP3.

IAPs are overly expressed in various cancers, enabling prolonged survival of cancerous cells [as reviewed by[49]]. Consequently, their antagonists are thought to either directly induce or sensitize cancerous cells to death by triggering proapoptotic pathways.[50,51] Interestingly, IAPs such as BIRC2 have recently been shown to be negative regulators of HIV transcription, and their expression is found to be correlated with viral latency.[23,31,32] Indeed, both BIRC2/3 and XIAP are overexpressed in HIV latently infected $CD4^+$ T and myeloid cells, and the SMs which induce the degradation of these IAPs can reactivate HIV. We demonstrate herein that various monovalent and bivalent SMs can induce efficient viral reactivation in different T cell models of latency and that some are more potent than others. Bivalent SMs are more effective than their monovalent counterparts, probably because of the presence of dimers that may contribute to a more stable and enhanced activation via interactions with the two adjacent binding domains of IAPs.[52] Among the bivalent SMs we examined, APG-1387 is most effective at degrading IAPs, facilitating a conversion of NFKB p100 to p52, and reactivating HIV expression through an NIK-dependent process, a hallmark of an activated non-canonical NFKB pathway.[23,24] In $CD4^+$ T cell models of HIV latency, APG-1387 treatment is associated with remarkable viral reactivation. However, in primary $CD4^+$ T cells infected with HI.fate.E dual reporter virus, exposure to APG-1387 is accompanied by a reduction in the frequency of latently infected cells (Figure 2) without a detectable change in the level of cells supporting LTR-directed transcription. The data suggest that the latent cells might be preferentially targeted for elimination without reactivation in contrast to PMA and ionomycin stimulation. This said, given the intrinsic properties of SMs, we cannot completely exclude the possibility that there was no change in the frequency of reactivated cells because latently infected cells rapidly die after reactivation.

Consistent with previous works with other SMs including AZD5582 [24] and ciapavir,[25] APG-1387 induces detection of viremia, albeit modestly, in ART-suppressed hu-mice as early as 48 h after treatment. Importantly, in mice treated with multiple doses of APG-1387, the proportion of cells carrying the integrated HIV DNA was meaningfully reduced, suggesting that the bivalent APG-1387 might preferentially target latently infected cells directly or indirectly for death (Figure 4). In addition, in APG-1387-treated mice the fact that the viral rebound was consistently lower throughout the ATI and plateaued at a level below pre-ART further strengthens the notion that APG-1387 impacts negatively the pool of VRs (Figure 6). It is conceivable that such an impact is significant considering the modest effect of APG-1387 on latency reversal in this experimental condition and the limited functional immune clearance mechanisms present in hu-BLT mice. This said, further experimentation with a larger group of animals analyzed at endpoint is needed to confirm the modulatory role of APG-1387 on VRs.

A more detailed analysis gauging the effect of APG-1387 on different $CD4^+$ T cell subsets revealed a potential modulation of splenic Th17-like cells and FOXP3-expressing $CD4^+$ T cells.

summary graphs showing results from multiple mice for each condition. Data are represented as median. Statistical analysis: two-tailed Mann-Whitney tests; ns, not significant (GraphPad Prism 8.0). The *p* values for the 'Stim' conditions were 0.11 for (A) and 0.41 for (B). In all relevant panels, each dot is one mouse ($n = 5$ for vehicle and $n = 4$ or 5 for APG-1387).

(C and D) Splenocytes from HIV-infected, ART-naïve mice were analyzed by flow cytometry for viral Gag p24 in Th-17-like and FOXP3-expressing $CD4^+$ T cells. The dot plot flow graphs in Panel C show the gating strategy to identify Th17-like ($CD3^+CD8^-IL17A^+$) or FOXP3-expressing ($CD3^+CD8^-FOXP3^+$) from human $CD45^+$ $CD19^-CD14^-$ cells in one mouse as an example. The graphs illustrate HIV-1 Gag p24-positive $IL17A^+$ $CD8^-$T cells or p24-positive $FOXP3^+$ $CD8^-$T cells expressing dim or no CD4. In Panel D, splenocytes isolated from HIV-infected, ART-naive mice ($n = 5$) were treated with APG-1387 (1 μM) *ex vivo* for up to 48h and stained for HIV-1 Gag p24. Splenocytes treated with vehicle control (VC) were used as a negative control. Depicted is the $p24^+$ cell count in total $CD4^+$ T cells, Th17-like and FOXP3-expressing T cells. Statistical analysis: two-tailed Wilcoxon paired rank tests; ns, not significant (GraphPad Prism 8.0). In (D), $p = 0.062$ for total $CD4^+$ T, $p > 0.99$ for Th17-like cells and $p = 0.62$ for $FOXP3^+$ cells. See also Figure S6.

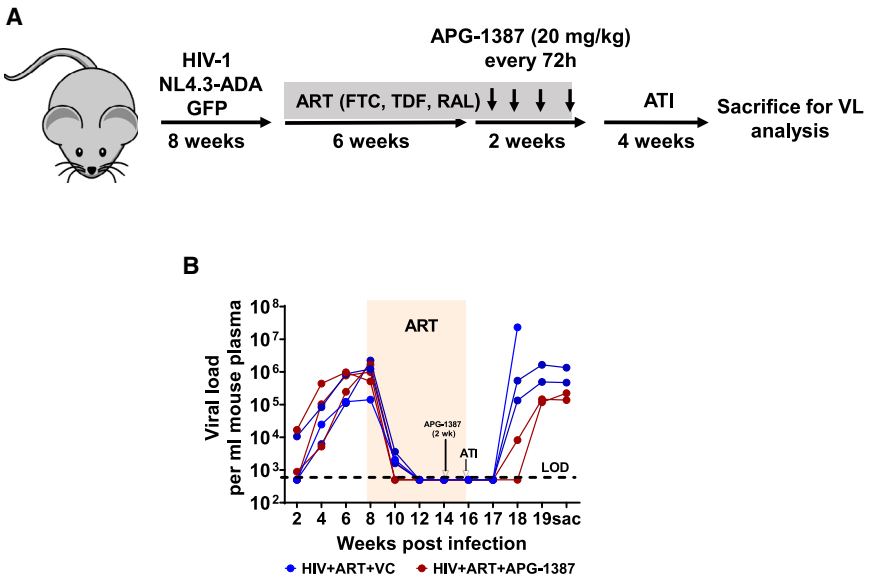

Figure 6. Sequential treatment of virally suppressed hu-BLT mice with APG-1387 reduced the level of viral rebound upon ART interruption

(A) Hu-BLT mice were infected with NL4.3-ADA-GFP and viral replication was suppressed by ART for 6 weeks. Mice were then treated with either APG-1387 or vehicle control for 2 weeks (4 doses) in the presence of ART. These mice were then subjected to a 4-week antiviral treatment interruption (ATI).

(B) Viremia of virally suppressed mice treated with VC ($n = 3$, blue lines) or APG-1387 ($n = 3$; red lines) was analyzed at regular intervals. Just before the sacrifice (sac) at 20 weeks post infection, we lost one mouse in each group. The orange background denotes the period of ART administration. The dotted line represents the limit of detection (LOD). Statistical analysis: non-parametric Kruskal-Wallis test ($p = 0.057$) followed by Dunn's multiple comparison test ($p > 0.999$), as analyzed using GraphPad Prism 8.0 software.

We observe a trend toward a reduction in Th17-cell frequency in both ART-suppressed mice treated *in vivo* with APG-1387 and in ART-naïve infected mice whose splenocytes were stimulated *ex vivo* with APG-1387 (Figure 5). Since Th17 cells have been proposed to be an important source of HIV latent reservoirs [reviewed in[53]], a decrease in Th17 cells might suggest a reduction in the level of integrated HIV DNA-harboring cells, an observation that was made with APG-1387 treated mice (Figure 4). Regarding FOXP3-expressing $CD4^+$ T cells in the spleen, there was no significant difference between ART-suppressed mice treated with APG-1387 or with the vehicle control. However, *ex vivo* stimulation of splenocytes from ART-naïve, HIV-infected mice with APG-1387 modestly decreased the number of p24-expressing $FOXP3^+$ $CD4^+$ T cells, although the difference was not statistically significant. Whether the non-canonical NFKB pathway is more functional in certain memory $CD4^+$ T cell subsets remains to be fully elucidated. The fact that the central memory subset has been shown to require strong TCR-mediated signaling for maintenance suggests a more important role of the canonical NFKB pathway in this context [reviewed in[26,54,55]]. Taken together, these results highlight the importance of evaluating the potential effects of SMs on various immune subsets known to be susceptible to HIV. Our study shows that APG-1387 has the capability to reactivate HIV, activate markers of apoptosis in latently infected cells, and reduce VRs without causing global T cell activation. However, the findings also underscore the need to combine bivalent SMs with other therapeutics to improve the reactivation and elimination of VRs. Indeed, recent findings have shown that combined panobinostat and pegylated interferon alpha 2 can transform the VR landscape through latency reversal and innate immune activation.[56]

Limitations of the study

Variations in the level of human cell reconstitution among mice, a common occurrence in this small animal model, may have contributed to different levels of effect by APG-1387. In addition, although the bivalent APG-1387 can decrease the frequency of virus-expressing Th17 and FOXP3-expressing $CD4^+$ T cells in hu-mice following *ex vivo* stimulation, the small number of mice per group and intrinsic differences between mice prevented us from reaching an irrefutable conclusion about the impact of APG-1387 on Th17 and FOXP3-expressing $CD4^+$ T cells in ART-suppressed hu-mice. In addition, potential differences in APG-1387 levels in different tissues might explain some of the disparities in the results. Also, the availability of the sex of the mice but not the sex of the fetal tissues prevents us from adequately assessing the potential sex-based effects with APG-1387 treatment. Lastly, in the experiments involving the use of $CD4^+$ T cells from healthy human donors, we did not have enough males and females studied, thus limiting the generalizability of the research findings. As well, an analysis of the influence of gender, ancestry, and ethnicity on the results of the study could not be established given the anonymity clause stipulated in the consent forms (human participants).

Another limitation of the study is the small number of mice available at endpoint to evaluate the modulation of VRs by APG-1387. Although hu-BLT mice remain the gold standard small animal model to conduct HIV cure research, it may not be the right system to investigate the effect of APG-1387 on microglia and long-lived resident macrophages that are derived from precursor cells in the yolk sac and thought to be potential sites of viral reservoirs. In addition, the immune system in hu-BLT mice does not fully recapitulate that of a human, thus limiting our ability to assess how infected cells are cleared in the context of APG-1387 treatment.

RESOURCE AVAILABILITY

Lead contact

Further information and requests for resources and reagents should be directed to and will be fulfilled by the lead contact, Éric A. Cohen (eric.cohen@ircm.qc.ca).

Materials availability

This study did not generate new unique reagents.

Data and code availability

- Data reported in this paper will be shared by the lead contact upon request.
- This paper does not report the original code.
- Any additional information required to reanalyze the data reported in this paper is available from the lead contact upon request.

ACKNOWLEDGMENTS

The following reagents were obtained through the NIH AIDS Reagent Program, Division of AIDS, NIAID, and NIH: ACH-2 cells from Dr. Thomas Folks (Cat # 349–443), TZM-bl cells, ARP-8129, contributed by Dr. John C. Kappes, Dr. Xiaoyun Wu and Tranzyme Inc. and J-Lat 10.6, ARP-9849, contributed by Dr. Eric Verdin. 2D10 was obtained from Dr. Jonathan Karn's lab (School of Medicine, Case Western Reserve University), and 2D10 NIK knock-out cells were a kind gift from Dr. Sumit K. Chanda (The Scripps Research Institute). We appreciate the technical support of the staff from the IRCM and CHU-Ste Justine Research Center animal facilities. We are grateful for the technical support provided by the IRCM flow cytometry platform. We are thankful to Robert Lodge, Isa Munoz Arias, and Mariana Bego for helpful discussions. We thank Mélanie Laporte and Olga Volodina for assistance with the animal work. Editorial assistance was provided by Ashutosh Pathak, Stephen Gutkin, Ndiya Ogba, and Paul Fletcher from Ascentage Pharma Group Inc. (Rockville, MD). The graphical abstract was created in BioRender. Cai, C. (2025) *https://BioRender.com/m63y853*. We thank all the blood donors and the IRCM clinic staff for their valuable contributions. This study was supported by the Canadian Institutes of Health Research (CIHR) grants FDN-154324 and HB2-164064 (Canadian HIV Cure Enterprise-CanCURE) to É.A.C. This work was also supported in part by the Fonds de Recherche du Québec - Santé-supported Réseau SIDA/Maladies Infectieuses. J.J. received postdoctoral fellowships from the CIHR HIV/AIDS priority program and FRQS. M.C.R.-M. is a recipient of a FRQS postdoctoral fellowship. S.B. was awarded a Richard and Edith Strauss postdoctoral fellowship in Medicine from McGill University. É.A.C. is the recipient of the IRCM-Université de Montréal Chair of Excellence in HIV Research. We dedicate this paper to the memory of co-author Dr. Natasha Patey, who passed away after the paper was accepted.

AUTHOR CONTRIBUTIONS

J.J. designed and performed experiments, analyzed/interpreted data, and wrote the manuscript. T.N.Q.P. designed and performed experiments, analyzed/interpreted data, wrote and revised the manuscript. S.B. assisted with hu-mouse work and performed experiments. M.C.R-M. assisted with hu-mouse work and data analysis, performed experiments, and generated the graphical abstract. N.B. assisted with experiments involving the dual reporter HIV vector and data analysis. Y.L. produced hu-BLT mice. F.D. provided overall technical support to the study and performed WB experiments. K.B. produced hu-BLT mice and critically reviewed the manuscript. N.P. and J.V.G. provided human fetal tissues. E.H. produced hu-BLT mice and critically reviewed the manuscript. Y.Z. provided APG-1387 and key pharmacological information about the molecule. E.A.C. designed experiments, analyzed data, wrote and revised the manuscript, and obtained funding. All authors reviewed and approved the manuscript prior to submission.

DECLARATION OF INTERESTS

Y.Z. is a full-time employee of Ascentage Pharma and an equity shareholder of Ascentage Pharma Group International, the parent company of Ascentage Pharma. All other authors declare no competing interests.

We, the authors, have a patent application related to this work.

STAR★METHODS

Detailed methods are provided in the online version of this paper and include the following:

SUPPLEMENTAL INFORMATION

Supplemental information can be found online at https://doi.org/10.1016/j.isci.2024.111470.

Received: June 21, 2024
Revised: August 22, 2024
Accepted: November 21, 2024
Published: November 27, 2024

REFERENCES

1. Chun, T.W., Moir, S., and Fauci, A.S. (2015). HIV reservoirs as obstacles and opportunities for an HIV cure. Nat. Immunol. *16*, 584–589. https://doi.org/10.1038/ni.3152.
2. Wong, M.E., Jaworowski, A., and Hearps, A.C. (2019). The HIV Reservoir in Monocytes and Macrophages. Front. Immunol. *10*, 1435. https://doi.org/10.3389/fimmu.2019.01435.
3. Kandathil, A.J., Sugawara, S., and Balagopal, A. (2016). Are T cells the only HIV-1 reservoir? Retrovirology *13*, 86. https://doi.org/10.1186/s12977-016-0323-4.
4. Colby, D.J., Trautmann, L., Pinyakorn, S., Leyre, L., Pagliuzza, A., Kroon, E., Rolland, M., Takata, H., Buranapraditkun, S., Intasan, J., et al. (2018). Rapid HIV RNA rebound after antiretroviral treatment interruption in persons durably suppressed in Fiebig I acute HIV infection. Nat. Med. *24*, 923–926. https://doi.org/10.1038/s41591-018-0026-6.
5. Siliciano, J.D., Kajdas, J., Finzi, D., Quinn, T.C., Chadwick, K., Margolick, J.B., Kovacs, C., Gange, S.J., and Siliciano, R.F. (2003). Long-term follow-up studies confirm the stability of the latent reservoir for HIV-1 in resting CD4+ T cells. Nat. Med. *9*, 727–728. https://doi.org/10.1038/nm880.
6. Margolis, D.M., Garcia, J.V., Hazuda, D.J., and Haynes, B.F. (2016). Latency reversal and viral clearance to cure HIV-1. Science *353*, aaf6517. https://doi.org/10.1126/science.aaf6517.
7. Deeks, S.G. (2012). HIV: Shock and kill. Nature *487*, 439–440. https://doi.org/10.1038/487439a.
8. Kim, Y., Anderson, J.L., and Lewin, S.R. (2018). Getting the "Kill" into "Shock and Kill": Strategies to Eliminate Latent HIV. Cell Host Microbe *23*, 14–26. https://doi.org/10.1016/j.chom.2017.12.004.
9. Tsai, A., Irrinki, A., Kaur, J., Cihlar, T., Kukolj, G., Sloan, D.D., and Murry, J.P. (2017). Toll-Like Receptor 7 Agonist GS-9620 Induces HIV Expression and HIV-Specific Immunity in Cells from HIV-Infected Individuals on Suppressive Antiretroviral Therapy. J. Virol. *91*, e02166-16. https://doi.org/10.1128/JVI.02166-16.
10. Wightman, F., Ellenberg, P., Churchill, M., and Lewin, S.R. (2012). HDAC inhibitors in HIV. Immunol. Cell Biol. *90*, 47–54. https://doi.org/10.1038/icb.2011.95.

11. Bashiri, K., Rezaei, N., Nasi, M., and Cossarizza, A. (2018). The role of latency reversal agents in the cure of HIV: A review of current data. Immunol. Lett. *196*, 135–139. https://doi.org/10.1016/j.imlet.2018.02.004.

12. Ait-Ammar, A., Kula, A., Darcis, G., Verdikt, R., De Wit, S., Gautier, V., Mallon, P.W.G., Marcello, A., Rohr, O., and Van Lint, C. (2019). Current Status of Latency Reversing Agents Facing the Heterogeneity of HIV-1 Cellular and Tissue Reservoirs. Front. Microbiol. *10*, 3060. https://doi.org/10.3389/fmicb.2019.03060.

13. Stoszko, M., Ne, E., Abner, E., and Mahmoudi, T. (2019). A broad drug arsenal to attack a strenuous latent HIV reservoir. Curr. Opin. Virol. *38*, 37–53. https://doi.org/10.1016/j.coviro.2019.06.001.

14. Garrido, C., Spivak, A.M., Soriano-Sarabia, N., Checkley, M.A., Barker, E., Karn, J., Planelles, V., and Margolis, D.M. (2016). HIV Latency-Reversing Agents Have Diverse Effects on Natural Killer Cell Function. Front. Immunol. *7*, 356. https://doi.org/10.3389/fimmu.2016.00356.

15. Walker-Sperling, V.E., Pohlmeyer, C.W., Tarwater, P.M., and Blankson, J.N. (2016). The Effect of Latency Reversal Agents on Primary CD8+ T Cells: Implications for Shock and Kill Strategies for Human Immunodeficiency Virus Eradication. EBioMedicine *8*, 217–229. https://doi.org/10.1016/j.ebiom.2016.04.019.

16. Zhao, M., De Crignis, E., Rokx, C., Verbon, A., van Gelder, T., Mahmoudi, T., Katsikis, P.D., and Mueller, Y.M. (2019). T cell toxicity of HIV latency reversing agents. Pharmacol. Res. *139*, 524–534. https://doi.org/10.1016/j.phrs.2018.10.023.

17. Rasmussen, T.A., and Lewin, S.R. (2016). Shocking HIV out of hiding: where are we with clinical trials of latency reversing agents? Curr. Opin. HIV AIDS *11*, 394–401. https://doi.org/10.1097/COH.0000000000000279.

18. Xing, S., and Siliciano, R.F. (2013). Targeting HIV latency: pharmacologic strategies toward eradication. Drug Discov. Today *18*, 541–551. https://doi.org/10.1016/j.drudis.2012.12.008.

19. Clutton, G.T., and Jones, R.B. (2018). Diverse Impacts of HIV Latency-Reversing Agents on CD8+ T-Cell Function: Implications for HIV Cure. Front. Immunol. *9*, 1452. https://doi.org/10.3389/fimmu.2018.01452.

20. Wong, L.M., and Jiang, G. (2021). NF-kappaB sub-pathways and HIV cure: A revisit. EBioMedicine *63*, 103159. https://doi.org/10.1016/j.ebiom.2020.103159.

21. Hiscott, J., Kwon, H., and Génin, P. (2001). Hostile takeovers: viral appropriation of the NF-kappaB pathway. J. Clin. Invest. *107*, 143–151. https://doi.org/10.1172/JCI11918.

22. Dave, R.S., Ali, H., Sil, S., Knight, L.A., Pandey, K., Madduri, L.S.V., Qiu, F., Ranga, U., Buch, S., and Byrareddy, S.N. (2020). NF-kappaB Duplications in the Promoter-Variant HIV-1C LTR Impact Inflammation Without Altering Viral Replication in the Context of Simian Human Immunodeficiency Viruses and Opioid-Exposure. Front. Immunol. *11*, 95. https://doi.org/10.3389/fimmu.2020.00095.

23. Pache, L., Dutra, M.S., Spivak, A.M., Marlett, J.M., Murry, J.P., Hwang, Y., Maestre, A.M., Manganaro, L., Vamos, M., Teriete, P., et al. (2015). BIRC2/cIAP1 Is a Negative Regulator of HIV-1 Transcription and Can Be Targeted by Smac Mimetics to Promote Reversal of Viral Latency. Cell Host Microbe *18*, 345–353. https://doi.org/10.1016/j.chom.2015.08.009.

24. Nixon, C.C., Mavigner, M., Sampey, G.C., Brooks, A.D., Spagnuolo, R.A., Irlbeck, D.M., Mattingly, C., Ho, P.T., Schoof, N., Cammon, C.G., et al. (2020). Systemic HIV and SIV latency reversal via non-canonical NF-kappaB signalling in vivo. Nature *578*, 160–165. https://doi.org/10.1038/s41586-020-1951-3.

25. Pache, L., Marsden, M.D., Teriete, P., Portillo, A.J., Heimann, D., Kim, J.T., Soliman, M.S.A., Dimapasoc, M., Carmona, C., Celeridad, M., et al. (2020). Pharmacological Activation of Non-canonical NF-kappaB Signaling Activates Latent HIV-1 Reservoirs In Vivo. Cell Rep. Med. *1*, 100037. https://doi.org/10.1016/j.xcrm.2020.100037.

26. Sun, S.C. (2017). The non-canonical NF-kappaB pathway in immunity and inflammation. Nat. Rev. Immunol. *17*, 545–558. https://doi.org/10.1038/nri.2017.52.

27. Oeckinghaus, A., and Ghosh, S. (2009). The NF-kappaB family of transcription factors and its regulation. Cold Spring Harbor Perspect. Biol. *1*, a000034. https://doi.org/10.1101/cshperspect.a000034.

28. Yu, H., Lin, L., Zhang, Z., Zhang, H., and Hu, H. (2020). Targeting NF-kappaB pathway for the therapy of diseases: mechanism and clinical study. Signal Transduct. Targeted Ther. *5*, 209. https://doi.org/10.1038/s41392-020-00312-6.

29. Creagh, E.M., Murphy, B.M., Duriez, P.J., Duckett, C.S., and Martin, S.J. (2004). Smac/Diablo antagonizes ubiquitin ligase activity of inhibitor of apoptosis proteins. J. Biol. Chem. *279*, 26906–26914. https://doi.org/10.1074/jbc.M313859200.

30. Campbell, G.R., and Spector, S.A. (2019). DIABLO/SMAC mimetics selectively kill HIV-1-infected resting memory CD4(+) T cells: a potential role in a cure strategy for HIV-1 infection. Autophagy *15*, 744–746. https://doi.org/10.1080/15548627.2019.1569950.

31. Campbell, G.R., To, R.K., Zhang, G., and Spector, S.A. (2020). SMAC mimetics induce autophagy-dependent apoptosis of HIV-1-infected macrophages. Cell Death Dis. *11*, 590. https://doi.org/10.1038/s41419-020-02761-x.

32. Campbell, G.R., Bruckman, R.S., Chu, Y.L., Trout, R.N., and Spector, S.A. (2018). SMAC Mimetics Induce Autophagy-Dependent Apoptosis of HIV-1-Infected Resting Memory CD4+ T Cells. Cell Host Microbe *24*, 689–702. https://doi.org/10.1016/j.chom.2018.09.007.

33. Li, N., Feng, L., Han, H.Q., Yuan, J., Qi, X.K., Lian, Y.F., Kuang, B.H., Zhang, Y.C., Deng, C.C., Zhang, H.J., et al. (2016). A novel Smac mimetic APG-1387 demonstrates potent antitumor activity in nasopharyngeal carcinoma cells by inducing apoptosis. Cancer Lett. *381*, 14–22. https://doi.org/10.1016/j.canlet.2016.07.008.

34. Pearson, R., Kim, Y.K., Hokello, J., Lassen, K., Friedman, J., Tyagi, M., and Karn, J. (2008). Epigenetic silencing of human immunodeficiency virus (HIV) transcription by formation of restrictive chromatin structures at the viral long terminal repeat drives the progressive entry of HIV into latency. J. Virol. *82*, 12291–12303. https://doi.org/10.1128/JVI.01383-08.

35. Jordan, A., Bisgrove, D., and Verdin, E. (2003). HIV reproducibly establishes a latent infection after acute infection of T cells in vitro. EMBO J. *22*, 1868–1877. https://doi.org/10.1093/emboj/cdg188.

36. Probst, B.L., Liu, L., Ramesh, V., Li, L., Sun, H., Minna, J.D., and Wang, L. (2010). Smac mimetics increase cancer cell response to chemotherapeutics in a TNF-alpha-dependent manner. Cell Death Differ. *17*, 1645–1654. https://doi.org/10.1038/cdd.2010.44.

37. Petersen, S.L., Peyton, M., Minna, J.D., and Wang, X. (2010). Overcoming cancer cell resistance to Smac mimetic induced apoptosis by modulating cIAP-2 expression. Proc. Natl. Acad. Sci. USA *107*, 11936–11941. https://doi.org/10.1073/pnas.1005667107.

38. Ratnapriya, S., Harris, M., Chov, A., Herbert, Z.T., Vrbanac, V., Deruaz, M., Achuthan, V., Engelman, A.N., Sodroski, J., and Herschhorn, A. (2021). Intra- and extra-cellular environments contribute to the fate of HIV-1 infection. Cell Rep. *36*, 109622. https://doi.org/10.1016/j.celrep.2021.109622.

39. Bellini, N., Lodge, R., Pham, T.N.Q., Jain, J., Murooka, T.T., Herschhorn, A., Bernard, N.F., Routy, J.P., Tremblay, C.L., and Cohen, É.A. (2022). MiRNA-103 downmodulates CCR5 expression reducing human immunodeficiency virus type-1 entry and impacting latency establishment in CD4(+) T cells. iScience *25*, 105234. https://doi.org/10.1016/j.isci.2022.105234.

40. Chen, Z., Chen, J., Liu, H., Dong, W., Huang, X., Yang, D., Hou, J., and Zhang, X. (2018). The SMAC Mimetic APG-1387 Sensitizes Immune-Mediated Cell Apoptosis in Hepatocellular Carcinoma. Front. Pharmacol. *9*, 1298. https://doi.org/10.3389/fphar.2018.01298.

41. Rizk, J., Kaplinsky, J., Agerholm, R., Kadekar, D., Ivars, F., Agace, W.W., Wong, W.W.L., Szucs, M.J., Myers, S.A., Carr, S.A., et al. (2019). SMAC mimetics promote NIK-dependent inhibition of CD4(+) TH17 cell differentiation. Sci. Signal. *12*, eaaw3469. https://doi.org/10.1126/scisignal.aaw3469.

42. Pan, W., Luo, Q., Yan, X., Yuan, L., Yi, H., Zhang, L., Li, B., Zhang, Y., Sun, J., Qiu, M.Z., and Yang, D.J. (2018). A novel SMAC mimetic APG-1387 exhibits dual antitumor effect on HBV-positive hepatocellular carcinoma with high expression of cIAP2 by inducing apoptosis and enhancing innate anti-tumor immunity. Biochem. Pharmacol. *154*, 127–135. https://doi.org/10.1016/j.bcp.2018.04.020.

43. Lee, G.Q., and Lichterfeld, M. (2016). Diversity of HIV-1 reservoirs in CD4+ T-cell subpopulations. Curr. Opin. HIV AIDS *11*, 383–387. https://doi.org/10.1097/COH.0000000000000281.

44. Rocco, J., Mellors, J.W., and Macatangay, B.J. (2018). Regulatory T cells: the ultimate HIV reservoir? J. Virus Erad. *4*, 209–214.

45. Ademe, M. (2020). Paradoxes in the Phenotype, Frequency and Roles of Myeloid-Derived Suppressor Cells During HIV Infection. HIV AIDS (Auckl) *12*, 151–156. https://doi.org/10.2147/HIV.S248642.

46. Zerbato, J.M., Purves, H.V., Lewin, S.R., and Rasmussen, T.A. (2019). Between a shock and a hard place: challenges and developments in HIV latency reversal. Curr. Opin. Virol. *38*, 1–9. https://doi.org/10.1016/j.coviro.2019.03.004.

47. Spivak, A.M., and Planelles, V. (2018). Novel Latency Reversal Agents for HIV-1 Cure. Annu. Rev. Med. *69*, 421–436. https://doi.org/10.1146/annurev-med-052716-031710.

48. French, A.J., Natesampillai, S., Krogman, A., Correia, C., Peterson, K.L., Alto, A., Chandrasekar, A.P., Misra, A., Li, Y., Kaufmann, S.H., et al. (2020). Reactivating latent HIV with PKC agonists induces resistance to apoptosis and is associated with phosphorylation and activation of BCL2. PLoS Pathog. *16*, e1008906. https://doi.org/10.1371/journal.ppat.1008906.

49. Dubrez, L., Berthelet, J., and Glorian, V. (2013). IAP proteins as targets for drug development in oncology. OncoTargets Ther. *9*, 1285–1304. https://doi.org/10.2147/OTT.S33375.

50. Fulda, S. (2017). Smac Mimetics to Therapeutically Target IAP Proteins in Cancer. Int. Rev. Cell Mol. Biol. *330*, 157–169. https://doi.org/10.1016/bs.ircmb.2016.09.004.

51. Fulda, S. (2015). Promises and Challenges of Smac Mimetics as Cancer Therapeutics. Clin. Cancer Res. *21*, 5030–5036. https://doi.org/10.1158/1078-0432.CCR-15-0365.

52. LaCasse, E.C., Mahoney, D.J., Cheung, H.H., Plenchette, S., Baird, S., and Korneluk, R.G. (2008). IAP-targeted therapies for cancer. Oncogene *27*, 6252–6275. https://doi.org/10.1038/onc.2008.302.

53. Renault, C., Veyrenche, N., Mennechet, F., Bedin, A.S., Routy, J.P., Van de Perre, P., Reynes, J., and Tuaillon, E. (2022). Th17 CD4+ T-Cell as a Preferential Target for HIV Reservoirs. Front. Immunol. *13*, 822576. https://doi.org/10.3389/fimmu.2022.822576.

54. Liu, T., Zhang, L., Joo, D., and Sun, S.C. (2017). NF-kappaB signaling in inflammation. Signal Transduct. Targeted Ther. *2*, 17023. https://doi.org/10.1038/sigtrans.2017.23.

55. Hovelmeyer, N., Schmidt-Supprian, M., and Ohnmacht, C. (2022). NF-kappaB in control of regulatory T cell development, identity, and function. J. Mol. Med. (Berl.) *100*, 985–995. https://doi.org/10.1007/s00109-022-02215-1.

56. Armani-Tourret, M., Gao, C., Hartana, C.A., Sun, W., Carrere, L., Vela, L., Hochroth, A., Bellefroid, M., Sbrolla, A., Shea, K., et al. (2024). Selection of epigenetically privileged HIV-1 proviruses during treatment with panobinostat and interferon-alpha2a. Cell *187*, 1238–1254. https://doi.org/10.1016/j.cell.2024.01.037.

57. Dave, V.P., Hajjar, F., Dieng, M.M., Haddad, É., and Cohen, É.A. (2013). Efficient BST2 antagonism by Vpu is critical for early HIV-1 dissemination in humanized mice. Retrovirology *10*, 128. https://doi.org/10.1186/1742-4690-10-128.

58. Vandergeeten, C., Fromentin, R., Merlini, E., Lawani, M.B., DaFonseca, S., Bakeman, W., McNulty, A., Ramgopal, M., Michael, N., Kim, J.H., et al. (2014). Cross-clade ultrasensitive PCR-based assays to measure HIV persistence in large-cohort studies. J. Virol. *88*, 12385–12396. https://doi.org/10.1128/JVI.00609-14.

59. Lodge, R., Lalonde, J.P., Lemay, G., and Cohen, E.A. (1997). The membrane-proximal intracytoplasmic tyrosine residue of HIV-1 envelope glycoprotein is critical for basolateral targeting of viral budding in MDCK cells. EMBO J. *16*, 695–705. https://doi.org/10.1093/emboj/16.4.695.

60. Schneider, C.A., Rasband, W.S., and Eliceiri, K.W. (2012). NIH Image to ImageJ: 25 years of image analysis. Nat. Methods *9*, 671–675. https://doi.org/10.1038/nmeth.2089.

61. Pham, T.N.Q., Meziane, O., Miah, M.A., Volodina, O., Colas, C., Béland, K., Li, Y., Dallaire, F., Keler, T., Guimond, J.V., et al. (2019). Flt3L-Mediated Expansion of Plasmacytoid Dendritic Cells Suppresses HIV Infection in Humanized Mice. Cell Rep. *29*, 2770–2782. https://doi.org/10.1016/j.celrep.2019.10.094.

62. Zhong, M.C., Lu, Y., Qian, J., Zhu, Y., Dong, L., Zahn, A., Di Noia, J.M., Karo-Atar, D., King, I.L., and Veillette, A. (2021). SLAM family receptors control pro-survival effectors in germinal center B cells to promote humoral immunity. J. Exp. Med. *218*, e20200756. https://doi.org/10.1084/jem.20200756.

STAR★METHODS

KEY RESOURCES TABLE

REAGENT or RESOURCE	SOURCE	IDENTIFIER
Antibodies		
Mouse anti-human CD3 (Clone OKT3)	BioLegend	Cat# 317330; RRID: AB_2563507
Mouse anti-human CD4 (Clone OKT4)	BioLegend	Cat # 317428; RRID: AB_21186122
Mouse anti-human CD8 (Clone SK1)	BioLegend	Cat# 344729; RRID: AB_2564509
Mouse anti-human CD8 (Clone SK1)	BioLegend	Cat# 344724; RRID: AB_2562790
Mouse anti-human HLA-DR (Clone L243)	BioLegend	Cat#307639; RRID: AB_11219187
Mouse anti-human CD14 (Clone M5E2)	BioLegend	Cat# 301833; RRID: AB_11126983
Mouse anti-human CD14 (Clone M5E2)	BioLegend	Cat# 301851; RRID: AB_2629575
Mouse anti-human CD14 (Clone M5E2)	BioLegend	Cat# 301822; RRID: AB_493747
Mouse anti-human IL17A (Clone eBio64DEC17)	Thermo Fisher Scientific	Cat# 25-7179-41; RRID: AB_11042972
Mouse anti-human FOXP3 (Clone 236A/E7)	Thermo Fisher Scientific	Cat# 12-4777-41; RRID: AB_1944448
Mouse anti-human CD45 (Clone 2D1)	BioLegend	Cat# 368526; RRID: AB_2687377
Rat anti-mouse CD45 (Clone 30-F11)	BioLegend	Cat# 103146; RRID: AB_2564003
Mouse anti-human CD69 (Clone FN50)	BioLegend	Cat# 310912; RRID: AB_314847
Mouse anti-human MKI67 (Clone B56)	BD Biosciences	Cat# 563757; RRID: AB_2688008
Rabbit anti-NFKB2 p100/p52 (18D10, Clone N/A)	Cell Signaling Technology	Cat# 3017S; RRID: AB_10697356
Rabbit anti-IKBA (Clone 44D4)	Cell Signaling Technology	Cat# 4812S; RRID: AB_10694416
Rabbit anti-BIRC2 (cIAP1) (Clone EPR4673)	Abcam	Cat# ab108361; RRID: AB_10862855
Rabbit anti-BIRC3 (cIAP2) (Clone E40)	Abcam	Cat# ab32059; RRID: AB_726890
Anti-actin beta HRP (Clone AC-15)	Abcam	Cat# ab49900; RRID: AB_867494
Rabbit anti-active CASP3 (caspase 3) (Clone C92-605)	BD Biosciences	Cat# 560626; RRID: AB_1727414
Mouse anti-human BCL2 (Clone 100)	BioLegend	Cat# 658708; RRID: AB_2563282
Mouse anti-human HIV-1 core antigen, KC57-FITC (Clone FH190-1-1)	Beckman Coulter	Cat# 6604665; RRID: AB_1575989
Goat anti-rabbit IgG H&L (HRP)	Abcam	Cat# ab205718; RRID: AB_2819160
Goat anti-mouse IgG (H + L)	Life Technologies	Cat# A-11001; RRID: AB_2534069
Bacterial and virus strains		
HIV: pNL4.3-ADA-GFP	Dave et al.[57]	N/A
HI.fate.E. dual reporter virus	Ratnapriya et al.[38]	N/A
Chemicals, peptides, and recombinant proteins		
APG-1387	Ascentage Pharma	N/A
Collagenase I	Sigma-Aldrich	Cat# C0130-1G
Collagenase XI	Sigma-Aldrich	Cat# C7657-1G
DNase (bovine pancreas)	Sigma-Aldrich	Cat# D4513-1VL
Hyaluronidase	Sigma-Aldrich	Cat# H3506-1G
Birinapant (TL32711)	AdooQ Bioscience	Cat# A12738-25
GDC-0152	Cayman Chemical	Cat# 17810
AT-406	Cayman Chemical	Cat# 19929
LCL-161	Cayman Chemical	Cat# 22420
Cremophor EL	Millipore Sigma	Cat# 238470
Polyethylene glycol 400	Sigma-Aldrich	Cat# 8074851000
Ionomycin calcium ionophore	STEMCELL Technologies	Cat# 73724
PMA	Sigma-Aldrich	Cat# P8139-1MG
PHA-L	Sigma-Aldrich	Cat# 11249738001

(*Continued on next page*)

Continued

REAGENT or RESOURCE	SOURCE	IDENTIFIER
Human IL2	Thermo Fisher Scientific	Cat# 200-02-100UG
Raltegravir potassium	APIChem	Cat# AC-2062
Emtricitabine	APIChem	Cat# AC-392
Tenofovir	APIChem	Cat# AC-5262
Efavirenz	Sigma-Aldrich	Cat# SML0536-10MG
Percoll	Sigma-Aldrich	Cat# GE17-0891-01
SuperScript II Reverse Transcriptase 10,000 U	Thermo Fisher Scientific	Cat# 18064014
Critical commercial assays		
COBAS AmpliPrep/COBAS TaqMan HIV-1 test (Version 2)	Roche	https://diagnostics.roche.com/
BD Cytofix/Cytoperm™ Fixation/ Permeabilization Solution Kit	BD Biosciences	Cat# 554722
BD Perm/Wash Buffer	BD Biosciences	Cat# 554723
FOXP3 transcription factor staining buffer set	Thermo Fisher Scientific	Cat# 00-5523-00
TaqMan Fast Advanced Master Mix	Thermo Fisher Scientific	Cat# 4444556
QIAzol Lysis Reagent	QIAGEN Sciences	Cat# 79306
Taq DNA polymerase with Standard Taq Buffer	New England Biolabs	Cat# M0273L
Lipofectamine 3000	Thermo Fisher Scientific	Cat# L3000015
ELISA MAX Standard Set Human TNF	BioLegend	Cat# 430201
ELISA MAX Deluxe Set Human IL6	BioLegend	Cat# 430504
Experimental models: Cell lines		
Human: ACH-2 cells (Sex of cells: Female)	NIH AIDS Reagent Program	Cat# ARP-349-443; RRID: CVCL_0138
Human: HEK293T (Sex of cells: Female)	ATCC	ATCC Cat# CRL-3216; RRID: CVCL_0063
Human: 2D10 (Sex of cells: Male)	Pearson et al.[34]	N/A
Human: 2D10 NIK knock-out (Sex of cells: Male)	Pache et al.[23]	N/A
Human: J-Lat 10.6 (Sex of cells: Male)	Jordan et al.[35]	Cat# ARP-9849; RRID: CVCL_8281
Human: Jurkat E6.1 (Sex of cells: Male)	ATCC	ATCC Cat# TIB-152; RRID: CVCL_0367
Human: TZM-bl (HeLa-derived) (Sex of cells: Female)	NIH AIDS Reagent Program	Cat#ARP-8129; RRID: CVCL_B478
Experimental models: Organisms/strains		
Mouse: NOD-*scid* IL2Rgammanull **NOD.Cg-*Prkdc*^{scid} *Il2rg*^{tm1Wjl}/SzJ**	The Jackson Laboratory	https://www.jax.org/strain/005557#; RRID: IMSR JAX:005557
Oligonucleotides		
Primer ULF1: ATG CCA CGT AAG CGA AAC TCT GGG TCT CTC TDG TTA GAC	Vandergeeten et al.[58]	N/A
Primer UR1: CCA TCT CTC TCC TTC TAG C	Vandergeeten et al.[58]	N/A
Primer HCD3OUT5': ACT GAC ATG GAA CAG GGG AAG	Vandergeeten et al.[58]	N/A
Primer HCD3OUT3': CCA GCT CTG AAG TAG GGA ACA TAT	Vandergeeten et al.[58]	N/A
Primer Alu1: TCC CAG CTA CTG GGG AGG CTG AGG	Vandergeeten et al.[58]	N/A
Primer Alu2: GCC TCC CAA AGT GCT GGG ATT ACA G	Vandergeeten et al.[58]	N/A
Primer Lambda T: ATG CCA CGT AAG CGA AAC T	Vandergeeten et al.[58]	N/A
Primer UR2: CTG AGG GAT CTC TAG TTA CC	Vandergeeten et al.[58]	N/A
Primer HCD3IN5': GGC TAT CAT TCT TCT TCA AGG T	Vandergeeten et al.[58]	N/A
Primer HCD3IN3': CCT CTC TTC AGC CAT TTA AGT A	Vandergeeten et al.[58]	N/A
Recombinant DNA		
psvCMV-VSV-G	Lodge et al.[59]	N/A

(*Continued on next page*)

Continued

REAGENT or RESOURCE	SOURCE	IDENTIFIER
Software and algorithms		
FACS Diva	BD Biosciences	https://www.bdbiosciences.com/en-us/products/software/instrument-software/bd-facsdiva-software
FlowJo (Versions 9.9.3 and 10.1)	TreeStar	https://www.flowjo.com/solutions/flowjo
ChemDraw	Revvity Signals	https://revvitysignals.com/products/research/chemdraw
Prism (Version 8.0)	GraphPad	https://www.graphpad.com
ImageJ	Schneider et al.[60]	https://github.com/imagej/ImageJ
Other		
Precision count beads	BioLegend	Cat # 424902

EXPERIMENTAL MODEL AND STUDY PARTICIPANT DETAILS

Hu-mice

The use of hu-BLT mice as a model to study HIV persistence and test therapeutic interventions was approved by the Center Hospitalier Universitaire (CHU) Sainte-Justine institutional (CER#2126) and the CSSS Jeanne-Mance review boards (Montreal, Canada), and applied in accordance with federal and provincial laws. Human fetal tissues were obtained following written informed consent to participate in this study. The sex of the fetal tissues was not available because it was either unknown to the donors or kept anonymous to experimenters as stipulated in the consent forms.

Hu-BLT mice were generated as previously reported.[61] In brief, male NOD-*scid* IL2Rgammanull (NSG, RRID:IMSR_JAX:005557) mice were purchased from the Jackson Laboratory (Bar Harbor, ME, USA) and housed in pathogen-free environment at CHU Sainte-Justine Research Center. NSG mice were subjected to total body irradiation with a sublethal dose (2.5 Gy) at 6–10 weeks of age. Irradiated mice were implanted with pieces of human fetal thymus fragments under the kidney capsule and received autologous fetal liver $CD34^+$ hematopoietic stem cells. Humanized mice were housed in germ-free facilities at CHU Sainte-Justine Research Center and Institut de recherches cliniques de Montréal (IRCM) under 12-h light-dark cycles, at room temperature with food and water *ad libitum*.

All animal experiments were approved by the IRCM Animal Care Committee (IRCM 2018-11) and by the CHU Sainte-Justine Animal Care and Use Committee (CIBPAR#2021–2961) following Good Laboratory Practices for Animal Research. Experimental procedures were performed in the BSL-3 Laboratory at the IRCM and conformed to the relevant regulatory standards in accordance with institutional and national guidelines. Fifty-six mice were used and data reported in this study (Table S2). The humanization age was between 10 and 15 weeks and the extent of human cell reconstitution (i.e., percentage of human $CD45^+$ cells in the blood at the start of the experiments) ranged between 24.6% and 97.3%. No randomization was performed; variations in the level of human $CD45^+$ cells between mice were evenly distributed among experimental groups. Exact details about the number of mice or tissues tested (sample size) in each experimental group were provided in appropriate Figure legends. No inclusion or exclusion criteria were applied.

Human subjects

Peripheral blood from anonymous healthy human donors were obtained after the participants had given written inform consent to participate in the study in accordance with the Declaration of Helsinki under research protocols approved by the IRCM Human Research Ethics Review Board (IRCM 2012-16). As per the terms of the consent forms, the blood donors remained anonymous to experimenters; thus, no information on the identity, age, ancestry, race, ethnicity, socioeconomic status or a combination of these factors could be obtained. Peripheral blood from 7 females and 3 males were used in the study, as described below and indicated on Figures or in the corresponding Figure legends. These 10 healthy subjects were used in three experiments and information related to the sample size and specific details for each experiment could be found in the Figure legends. The absence of sex-based analyses limits the generalizability of some of the findings in this study and this is highlighted under Section 'Limit of Study'. An analysis of the influence of gender, ancestry, ethnicity on the results of the study could not be performed given the anonymity clause of the consent forms.

Cell lines

The HEK 293T cell line (RRID:CVCL_0063), obtained from the American Type Culture Collection (ATCC) is a derivative of the human embryonic kidney (HEK) 293 cell line which was generated from the kidney of an aborted female fetus. The TZM-bl (RRID:CVCL_B478), obtained from the NIH AIDS Reagent Program, was generated from a female with cervical carninoma. The ACH-2

cell line (RRID:CVCL_0138), obtained from the NIH AIDS Reagent Program, was from a four-year-old female with T acute lymphoblastic leukemia. The Jurkat E6.1 cell line (RRID:CVCL_0367), obtained from the ATCC, came from a 14-year-old male with acute T cell leukemia. The 2D10, 2D10 NIK-knockout and J-Lat 10.6 (RRID:CVCL_8281) cell lines were all derived from the parental Jurkat E6.1 cell line mentioned above.

All cell lines were cultivated in DMEM (HEK 293T and TZM-bl) or RPMI-1640 media (ACH-2 and all Jurkat-based cell lines) supplemented with 10% fetal bovine serum (FBS) at 37^0C in incubators supplied with 5% CO_2 in air atmosphere. All cell lines were routinely checked in our laboratory and confirmed to be mycoplasma-free. No other information related to cell authentication was available.

Primary cell cultures from hu-mice

Primary cells were isolated from blood and tissues of hu-mice (all males) described in the preceding Section entitled 'Hu-mice'. Cells were used in experiments approved by the IRCM Animal Care Committee (IRCM 2018-11) and by the CHU Saint-Justine Animal Care and Use Committee (CIBPAR#2021–2961). All experimental procedures conformed to the relevant regulatory standards in accordance with the institutional and national guidelines. The sex of human cells in hu-mice was not available since the sex of human fetal tissues used to generate the animals was either unknown to the donors or kept confidential in accordance with the terms of the consent forms. Cells isolated from tissues of hu-mice were cultivated in RPMI-1640 media supplemented with 10% FBS at 37^0C in incubators supplied with 5% CO_2 in air atmosphere.

Primary cell cultures from human subjects

$CD4^+$ T cells were purified from peripheral blood of 7 female and 3 male healthy subjects whose blood was drawn after the participants had given written inform consent in accordance with the Declaration of Helsinki under research protocols approved by the IRCM Human Research Ethics Review Board (IRCM 2012-16). $CD4^+$ T cells were used in the experiments shown in Figures 2, S2, and S3. Precise usage of the donors was indicated on the Figures or in the corresponding Figure legends. $CD4^+$ T cells, grown in RPMI-1640 media supplemented with 10% FBS, were cultivated at 37^0C in incubators supplied with 5% CO_2 in air atmosphere.

METHOD DETAILS

Experimental design

No randomization and/or stratification was performed. Hu-mice with variable levels of human $CD45^+$ cells were equally distributed among experimental groups. All efforts were made to have equal or comparable number of mice or samples (i.e., number of n) per experimental group or condition. The exact number of n was provided in relevant Figure legends. Experimenters were blinded during processing biological samples, conducting experiments and analyzing samples in different assays. No inclusion or exclusion criteria were applied to the study. No statistical methods were used to pre-determine strategies for randomization and/or stratification, population size, inclusion and exclusion of any data or subjects, or whether the data met assumptions of the statistical approach.

Pharmacological and toxicity analysis

Hu-BLT mice were left untreated or treated via intraperitoneal route (IP) with either vehicle- (10% sterile Cremophor dissolved in 5% polyethylene glycol-400 and 85% PBS) or 20 mg/kg (100 APG-1387 (Ascentage Pharma, China) every third day (maximum 100 μL injection volume) for up to 4 weeks. Plasma was collected at different intervals and white blood cells isolated by treating whole blood with red blood cell lysis buffer (Invitrogen, U.S.A). Cells from blood and tissues were analyzed by flow cytometry as described in Section 'flow cytometry' below for the effect of APG-1387 on cell proliferation and activation. Proinflammatory cytokines were evaluated in plasma of healthy untreated, APG-1387- and vehicle-treated hu-BLT mice using Legend Max enzyme-linked immunosorbent assay (ELISA) kits for human TNF and IL6 (both from BioLegend, U.S.A) as per the manufacturer's protocol. Data analysis was performed using GraphPad Prism software (Version 8.0).

HIV infection and ART treatment of hu-mice

Stocks of HIV-1 NL4.3-ADA-GFP were prepared and titered as previously reported.[57] In brief, HEK293T cells ($5x10^6$) were transfected with 25 μg CCR5-tropic HIV pNL4.3-ADA-GFP using the calcium phosphate method. Culture supernatant was collected 48h later and virus was concentrated by ultracentrifugation over a 20% sucrose gradient. The pelleted virus was resuspended in DMEM media and titrated in TZM-bl cells to determine 50% tissue culture infectious units ($TCID_{50}$).[61] $TCID_{50}$ values were calculated using the Spearman-Karber method. Hu-BLT mice were inoculated by IP (in 100 μL volume) twice (24-h apart) with 100,000 $TCID_{50}$ each. Plasma HIV viral load was determined every 1–2 weeks using the quantitative COBAS AmpliPrep/COBAS TaqMan HIV-1 test, Version 2.0 (detection limit, 20 copies/ml; Roche Diagnostics, U.S.A).

After viral peak was reached (6–8 weeks post infection), mice were subjected to a daily ART regimen containing emtricitabine (100 mg/kg), tenofovir disoproxil fumarate (50 mg/kg), and raltegravir (68 mg/kg) via subcutaneous injections (maximum volume 120 μL). The three compounds were obtained from APIChem Technology (Zhejiang, China). Subsequently, virally suppressed mice were treated for up to 2 weeks with APG-1387 (20 mg/kg, every third day) or vehicle via the IP route as described in Section 'Pharmacological and toxicity analysis' above. In the experiment where mice received more than one doses of APG-1387, ART was maintained during the two-week treatment with APG-1387. In some cases, virally suppressed mice, treated or not with

APG-1387, were subjected to a 4-week ATI after APG-1387 treatment. For experiments which aimed to assess the effect of APG-1387 *ex vivo*, infected mice were not treated with ART or APG-1387 at anytime leading up to the endpoint of the experiment (euthanasia).

Cell isolation from blood and tissues

Hu-BLT mice were euthanized by gas (isoflurane) anesthesia overdose and intracardiac puncture according to institutional protocols approved by the IRCM Animal Care Committee. Euthanasia was done between 4 and 20 weeks after initiation of the experiment. Cardiac perfusion was performed before tissues were harvested using PBS containing 20 IU/mL heparin. Bone marrow cells were isolated from the femur as described.[62] Briefly, femurs were removed and residual tissues excised from the bones before the cavities were flushed with PBS-2% FBS to recover bone marrow cells. Cells from the spleen, lung and liver were isolated as reported previously.[61] In brief, spleen was crushed and passed through a 40-μm cell strainer to obtain single-cell suspensions (BD Biosciences). Lung and liver tissues were digested with a mixture of enzymes (all from Sigma-Aldrich) containing 1350 U collagenase I, 37.5 U collagenase XI, 18 U hyaluronidase and 7.2 U DNase in 2 mL HBSS for 1h at 37°C. Cell suspension was filtered through a sterile 70-μm cell strainer, and cells purified by centrifugation (870 x *g*) over a 40%–80% Percoll (Sigma-Aldrich) gradients. In all cases, cells were washed with PBS and contaminating red blood cells (RBCs) were removed using RBC lysis buffer (PBS containing 0.8% ammonium chloride).

Ex vivo stimulation of splenocytes

In certain experiments, spleen cells from virally suppressed, vehicle-treated or APG-1387-treated hu-mice were seeded in a 96 U-bottom well plate (0.5–1 million cells) with 200 μL RPMI-1640 media (+10% FBS) and stimulated with PMA (5 ng/mL) and ionomycin (500 ng/mL). Cells treated with vehicle control (DMSO) were used as negative controls. Twenty-four hours later, they were analyzed for IL17A-producing (Th17-like) or FOXP3-expressing $CD4^+$ T cells using flow cytometry as described below. Alternatively, spleen cells from HIV-infected, ART-naïve mice were treated APG-1387 (1 μM) or vehicle (DMSO) for 48h and analyzed by flow cytometry as described below for the frequency of total $CD4^+$ T-, Th17-like- or $FOXP3^+$ $CD4^+$ T-expressing the HIV Gag p24 protein.

$CD4^+$ T cell infection with single-round HIV

HEK293T cells (5×10^6) were transfected with 20 μg of HI.fate.E dual reporter proviral DNA[38] and pseudotyped with 8 μg psvCMV-VSV-G,[59] using Lipofectamine 3000 Transfection Reagent as per manufacturer's instructions (Thermo Fisher Scientific). The HI.fate.E dual reporter lentiviral vectors were concentrated by ultracentrifugation over a 20% sucrose cushion and titered in Jurkat E6.1 cells. The proportion of infected cells supporting viral replication, designated replicating (E2-CRMZ-positive cells) was used to estimate infectious units.

$CD4^+$ T cells were isolated from peripheral blood mononuclear cells using $CD4^+$ T cell isolation kit (Miltenyi Biotec, USA) and activated with phytohemagglutinin-L (10 μg/mL, Sigma-Aldrich) in the presence of IL2 (100 U/ml, Peprotech, USA). Thereafter, cells were transduced with HI.fate.E dual reporter virus at multiplicity of infection-1 (MOI-1). To confirm the authenticity of transduction, $CD4^+$ T cells were treated with 5 μM efavirenz (EFV, Sigma-Aldrich) for 2 h before viral inoculation. At 72 h post transduction, cells were treated with varying concentrations of APG-1387 (0.1–10 μM) or vehicle (DMSO) for 24 h. Transduced primary $CD4^+$ T cells treated with PMA/ionomycin, which activates the canonical NFKB pathway, were used as controls. Frequencies of cells supporting viral replication (replicating) and latently infected $CD4^+$ T cells were determined by flow cytometry.

HIV reactivation from latent cells

Jurkat-based cell lines J-Lat 10.6 [35], 2D10 [34] and 2D10 NIK knock-out[23] were seeded at 20,000 cells (100 μL) in a 96-well plate and treated for up to 48 h with APG-1387 or other SMs including GDC-0152, AT-406, LCL-161 and Birinapant from as low as 0.01 pM up to 10 μM. Cells treated with vehicle (DMSO) were used as controls. Samples were fixed and acquired on SA3800 Spectral Analyzer (Sony Biotechnology) or BD LSRFortessa Cell Analyzer with FACS Diva software (BD Bioscience). These Jurkat-based cell lines contain an HIV-1 genome that expresses GFP upon activation. Thus, reactivation of $CD4^+$ T cell models of latency was determined by measuring the percentage of GFP^+ cells after treatment. Results were analyzed using FlowJo (Versions 9.9.3 and 10.1; FlowJo LLC, BD Life Sciences).

Flow cytometry

Cells from blood and/or tissues were stained with fluorescently labeled Abs against mouse CD45 along with those specific for human CD45, CD3, CD4, CD8, CD14, CD69 and HLA-DR as required for the experiments. When appropriate, surface-stained cells were fixed and permeabilized using the BD Cytofix/Cytoperm solution kit and BD Perm/Wash buffer (BD Biosciences) as per the manufacturer's instructions and intracellularly stained for HIV-Gag p24 using anti-human HIV-1 core antigen, KC57-FITC (Beckman Coulter, USA), and/or cytoplasmic proteins of interests using appropriate Abs (e.g., anti-active CASP3, anti-human BCL2). In some cases, permeabilization was done using a FOXP3/Transcription Factor Staining kit (eBioscience, USA) to stain for ILT17 using anti-human IL17A Ab or nuclear-like proteins including FOXP3 and marker of proliferation marker Ki-67, MKI67 using anti-human FOXP3 and anti-human MKI67 Abs, respectively. The full Ab list used for flow cytometry analysis can be found in the

key resources table. When appropriate, precision counting beads (BioLegend, USA) were used to determine the cell count. Samples were acquired on a BD LSRFortessa Cell Analyzer (BD Bioscience) using FACSDiva software and analyzed by FlowJo (Versions 9.9.3 and 10.1).

Western blotting

Cells were washed with phosphate-buffered saline (PBS) and then lysed using radioimmunoprecipitation assay RIPA buffer (1% NP-40, 140 mM NaCl, 0.05% SDS, 5 g/L Na-Deoxycholate, 8 mM Na_2HPO_4 and 2 mM NaH_2PO_4, pH 7.2) for 20 min at 4°C. Immunoblotting was performed according to standard protocols.[24] Primary Abs such as α-NFKB2 p100/p52, α-IKBA, α-BIRC2, α-BIRC3 and α-ACTB, were added to protein immunoblots and incubated overnight at 4 °C. Protein signals were detected with appropriate secondary Abs including an anti-rabbit Ab. Quantification of protein signals on Western blots was done using ImageJ software.[60] Information about the Abs used in Western blotting can be found in key resources table.

Nucleic-acid extraction and qPCR

RNA from all lymphoid and non-lymphoid tissues were extracted using QIAzol Lysis Reagent (QIAGEN Sciences, USA) according to manufacturer's instructions and analyzed using previously published protocols.[61] RNA was reverse transcribed using SuperScript II RT (Thermo Fisher Scientific, U.S.A). Total DNA from tissue-derived cells was extracted using the QIAamp DNA mini kit (QIAGEN Sciences, U.S.A) according to manufacturer's instructions. HIV DNA was quantitated as described previously.[58] In brief, preamplification of total DNA was done using 4 primers (300 nM each) ULF1, UR1, HCD3OUT5′ and HCD3OUT3′, while that for integrated DNA was done using ULF1 (150 nM) and 300 nM each of Alu1, Alu2, HCD3OUT5′ and HCD3OUT3'. The second round PCR were performed in real time using ViiA 7 Real-Time PCR system using TaqMan Fast Advanced Master Mix (Thermo Fisher Scientific, U.S.A). The primers are Lambda T and UR2 (both at 1250 nM) for total and integrated HIV DNA. Primers HCD3IN5′ and HCD3IN3′ are for the amplification of the CD3 gene (2 copies per cell) and used to determine the exact number of cells in the reaction.[58] DNA from serially diluted ACH-2 cells (NIH HIV Reagent Program) was extracted and amplified in parallel to generate a standard curve from which unknown samples were enumerated.

QUANTIFICATION AND STATISTICAL ANALYSIS

Flow cytometry data were analyzed using FlowJo (Versions 9.9.3 and 10.1). Quantification of Western blots was performed using ImageJ software. Data analysis and presentation was done using GraphPad Prism (Version 8.0). Experimenters were blinded during data analysis of samples.

Descriptive measures (mean, median, minimum/maximum range, 95% confidence intervals, and percent) were used to summarize the data and illustrate in graphical presentations. All statistical analysis was done using GraphPad Prism (Version 8.0). Nonparametric (unpaired) Mann-Whitney's U-test (two-tailed) was conducted to compare ranks between two experimental groups (e.g., treated with vehicle or with APG-1387). Nonparametric (paired) Wilcoxon test was performed to compare the ranks of two matched samples (e.g., before and after treatment with APG-1387). When comparing multiple groups, non-parametric tests Kruskal-Wallis or Friedman were performed and followed by Dunn's multiple comparison test (e.g., vehicle-treated group compared to those treated with different concentrations of APG-1387 or combined PMA and ionomycin; effect of APG-1387 on viral rebound at different time points post treatment interruption). A p value of less than 0.05 was considered statistically significant. ns, *, **, ***, signify not significant, <0.05, <0.01, and <0.001, respectively. Accordingly, in the non-parametric Friedman test followed by Dunn's multiple comparisons test shown in Figure 2, the exact p values were $^{*}p = 0.026$, $^{**}p = 0.007$, $^{***}p = 0.0004$. In the two-tailed Mann-Whitney unpaired rank test shown in Figure 3, the $^{*}p$ value was 0.0286 while in Figure 4, the p values were as follows: $^{*}p = 0.0317$ and $^{**}p = 0.0043$. For Figure S6, the $^{*}p$ value was <0.05.

No statistical methods were used to pre-determine strategies for randomization and/or stratification, population size, inclusion and exclusion of any data or subjects, or whether the data met assumptions of the statistical approach. All software used in data analysis along with statistical parameters were mentioned in the appropriate Figure legends. Details about the statistical tests, exact values of n and definitions of the n were as indicated in the legend for each relevant Figure. When applicable, definition of asterisks and descriptive measures were indicated in the Figure legends or Results.

Drawing of the chemical structure of APG-1387 shown in Figure 1 was done using the ChemDraw software.